Report for the final year project entitled:

Adhesive wear of rubber in mining application under dry contact condition

Submitted by:

Hamad Almuhaini

November 2019

Table of Contents

Chapter 1. Introduction 8
1.1 Wear in mining applications 8
1.2 Project specifications 11
1.2.1 Project aim 11
1.2.2 Timelines 12
1.2.3 Risk assessment 13
1.2.4 Resource plan 14
1.3 Dissertation organization 15
Chapter 2. Literature review 16
2.1 Introduction 16
2.2 Wear mechanisms 16
2.2.1 Adhesive wear 20
2.2.2 Abrasive wear 25
2.3 Standard tests for wear of rubber 29
2.3.1 Adhesive wear 29
2.3.2 Abrasive wear 34
2.4 Laboratory tribo-test machine 38
2.5 Wear process 40
2.6 Adhesive wear 42
2.7 Abrasive wear 45
Chapter 3. Methodology 53
3.1 Introduction 53
3.2 Experimental procedure 56
3.3. Scanning electron microscope (SEM) observations 58
Chapter 4. Results and discussions 59
4.1 Introduction 59
4.2 Measured data 59
4.3 Adhesive wear plots 63
4.3.1 Speed of 2.2 m/s 63

4.3.2 Speed of 2.6 m/s 65
4.3.3 Speed of 3 m/s 67
4.3.4 Results comparison 69
4.4 SEM observations 71
Chapter 5. Conclusions 73
References 75

List of figures

Figure 1.1. A conveyor belt system (Hakami et al., 2017) 10
Figure 2.1 Classification of wear (Sasaki et al., 2013) 15
Figure 2.2. Schematics of different wear mechanisms (Sasaki et al., 2013) 17
Figure 2.3. Material removal in adhesive wear (Tanzi et al., 2019) 19
Figure 2.4. Adhesive wear process, (a) thin flake-like wear particle (b) wedge-like wear particle (Kayaba and Kato, 1981) (Sasaki et al., 2013) 20
Figure 2.5. Abrasive wear: (a) two body, (b) three body (Hakami et al., 2017) 24
Figure 2.6. Pattern for abrasion in a sample test rubber (Hakami et al., 2017) 25
Figure 2.7. Needle trace on the rubber surface generated by different normal load (Wu, 2017) 26
Figure 2.8. A schematic of stress concentration and strain distribution of the surface of the rubber around the tip of the needle (Wu, 2017) 27
Figure 2.9. ASTM D429 method C (Applerubber, 2019) 29
Figure 2.10. ASTM D413 test (Mecmesin, 2018) 30
Figure 2.11. ASTM G77 standard test for adhesive wear (coatings, 2019) 31
Figure 2.12. Schematic diagram of the ISO 4649 test device 33
Figure 2.13. Abrasion wear test machine TR-50. (a) photograph of the machine, (b) schematic of the interior components (Singh, 2016) 34
Figure 2.14. ASTM G 174 abrasion test; A is the specimen and B is the moving strip (Budinski and Budinski, 2017) 34
Figure 2.15. Schematic drawing showing the most common configurations of tribological machine for adhesive and abrasive testing. (a) block on disc (BOD), (b) block on ring (BOR) and (c) dry sand rubber wheel (DSRW), (Yousif, 2013) 37
Figure 2.16. Multi-functional tribo-test machine (Alshammari et al., 2018) 38
Figure 2.17. Schematic of the modified tests, (a) ISO 4649 and (b) ASTM G65 (Molnar et al., 2018) 48
Figure 3.1. Schematic of testing machine used for experimental tests in this thesis (Yousif, 2013) 54
Figure 3.2. Photograph of the testing machine for adhesive test under contact condition (Yousif, 2013) 56
Figure 3.3. Rubber specimen in the testing machine 57
Figure 3.4. Rubber specimen; (a) before experiment, (b) after experiment 58
Figure 4.1. Distance vs. volume loss for speed 2.2 m/s 63
Figure 4.2. Distance vs. specific wear rate for speed 2.2 m/s 64
Figure 4.3. Distance vs. average friction coefficient for speed 2.2 m/s 64
Figure 4.4. Distance vs. volume loss for speed 2.6 m/s 65
Figure 4.5. Distance vs. specific wear rate for speed 2.6 m/s 66

Figure 4.6. Distance vs. average friction coefficient for speed 2.6 m/s 66
Figure 4.7. Distance vs. volume loss for speed 3 m/s 67
Figure 4.8. Distance vs. specific wear rate for speed 3 m/s 68
Figure 4.9. Distance vs. average friction coefficient for speed 3 m/s 68
Figure 4.10. Distance vs. volume loss for different speeds at normal load of 20 N 70
Figure 4.11. Distance vs. specific wear rate for different speeds at normal load of 20 N 70
Figure 4.12. Distance vs. average friction coefficient for different speeds at normal load of 20 N 71
Figure 4.13. SEM micrographs of the rubber sample..... 70

List of tables

Table 1.1. Timelines of the project 10
Table 1.2. Risk assessments and treatments 11
Table 3.1. Specifications of the testing machine (Yousif, 2013) 55
Table 4.1. Measured data for speed 2.2 m/s 60
Table 4.2. Frictional force for speed 2.2 m/s 60
Table 4.3. Measured data for speed 2.6 m/s 61
Table 4.4. Frictional force for speed 2.6 m/s 61
Table 4.5. Measured data for speed 3 m/s 62
Table 4.6. Frictional force for speed 3 m/s 62

Abstract

Wear in rubber materials is one of the important fault factors in which the object loses its efficiency due to the gradual removal of its material. It occurs frequently if the rubber material is under load or stress and imposes significant economic costs on the industries with repair or maintenance. As a result, study of wear process in rubbers is required to obtain more information about the wear and the factors which affect this process.

Wear in rubbers are categorized into different types. Two important ones are abrasive and adhesive wear which can happen under dry and wet contact conditions. In this research study, both wearing processes are first investigated and then the results of adhesive wear tests on a rubber material under dry contact condition are presented.

Different tests were performed on a rubber material in this research work to measure wear parameters such as volume loss, specific wear rate and average friction coefficient. The tests were performed for speeds of 2.2, 2.6 and 3 m/s to generate different sliding distance. Different normal loads of 10, 20, 30 and 40 N were also applied on the sample to investigate the effects of normal load on the wear parameters.

The obtained results show that the wear parameters including volume loss, specific wear rate and average friction coefficient are significantly affected by the test speed, normal load and sliding distance.

Chapter 1. Introduction

This chapter presents basic concepts of wear which happens especially on rubbers and in the cases of mining application. It first provides basic explanations of wear and tribology and then presents some information about the wear in mining applications. At the end, a detailed discussion about different types of wear in rubbers and wear mechanisms is given.

Wear is generally defined as the gradual removal or deformation of material at solid surfaces due to mechanical reasons such as erosion or chemical reasons such as corrosion. The study of wear mechanism and other related processes is referred to tribology. Tribology is defined as the science of interacting surfaces in relative motion. It consists of the interactions between solids or between solids and liquids or gases. Tribology includes all aspects of friction and wear with or without lubrication (Kovaříková et al., 2009).

Wear occurs in two surfaces named the base body and counter body as soon as they come into contact. Particularly it increases when there is no lubrication between two surfaces in contact or when the lubrication film thickness becomes thin. Wear is a continuous loss of material from the surface of a solid due to mechanical reasons by contact and relative motion of a solid body. Wear can be recognized by presence of small detached particles or removal of material of two contacted bodies (Kovaříková et al., 2009).

1.1 Wear in mining applications

The world population has started increasing significantly since the last decades and this has increased the demand for the global energy. In addition, a high percentage of this population have settled in big cities where there are several factories and industries which needs different

types of energy. The traditional sources of energy mostly come from fossil fuels such as coal, oil and natural gas. Although a small part of energy resources come from the renewable energies (Holmberg et al., 2017).

Mining is a processing for finding coal and other solid minerals as a main part of energy resources around the world. This is a fundamental part of human activity which dates back to thousands years ago to search for raw materials by excavation or extraction. In addition to search for coal and solid minerals, mining also is the activity for finding the others needs and more valuable in some cases such as diamond, gold, silver, iron and copper.

One of the main devices for transportation of raw materials in mining is the conveyor belt. This kind of systems can carry bulk materials obtained from the excavation in different sizes and variety of weighs in continuous or semi-continuous mode. The length of the conveyor belt used in mining can be varied from few meters or several kilometers. The length of conveyor belt used for transporting phosphates in Bou Craa mine in Africa is up to 98 kilometers (Molnar et al., 2018).

The belt used in a conveyor system is usually made of rubber which is one of the most important materials used for engineering applications. Rubber is very stretchable with a high value of elasticity which can absorb energy to a significant level. Nowadays, different types of rubber are used in for various applications in industry.

Figure 1.1 shows a different parts of a conveyor belt system which consists of at least two pulleys or more (depends on the length of the belt) and a belt to carry the raw materials in mines. The material of the belt is mainly of polymers such as PVC or rubbers depending on the type of applications. Rubbers has some useful properties such as low Young modulus, high Poisson ratio

and high yield strain. Figure 1(c) presents different layers of a cross section of belt used in conveyor systems. As it is shown, a belt consists of three layers; top cover rubber, coating rubber and bottom cover rubber (Hakami et al., 2017).

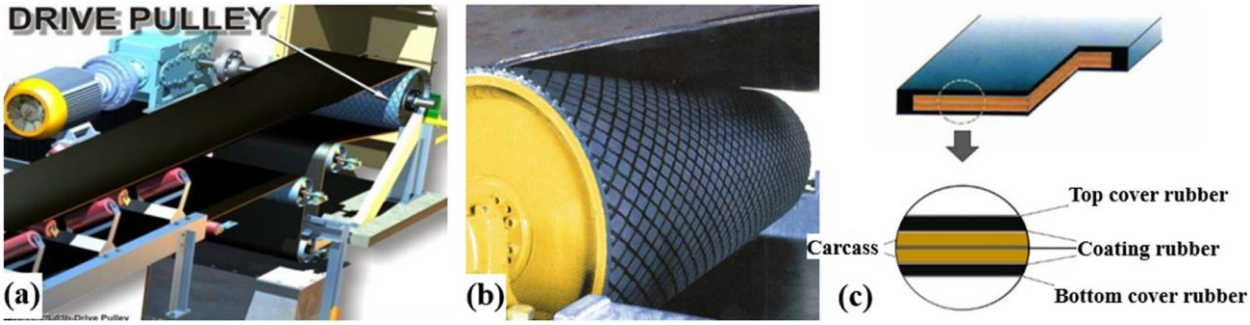

Figure 1.1. A conveyor belt system (Hakami et al., 2017)

The top layer is used in the belt to make it resistance against wear. The middle layer which is made of carcass material is to provide adhesion between the rubber and carcass and also the tensile strength for the belt. The role of bottom layer is to cover the middle carcass layer and provide enough roughness and friction between the belt and surface of pulley to drive it. The top layer should be of the main focus in design since it is more in contact with the loads and stresses and should tolerate the wear process.

The belt in a conveyor system should tolerate different kinds of stress during the system operation including normal stress, bending stress and tensile stress when carrying the raw materials, rolling stress when rotating around the pulleys. In addition, it is subjected to wear and friction during the service life. There are two main reasons of wearing in the belt during the operation; at the loading point of bulk material transportation which leads to wearing the belt in

the center. The second source of wear in the belts is the scrapers which is originally used to clean the belt from the tiny raw materials which is left on the conveyor belt during the operation. However, it is claimed that about one third of the damage on the worn belt is due to unsuitable use of scrapers for cleaning the belt (Molnar et al., 2018).

Since the conveyor belt system includes some moving parts and components, the associated wear and friction on them impose some costs together with maintenance for the system. Usually, replacement of the worn component especially for the belt happens with a significant amount of cost and time. However, this kind of transportation system (conveyor belt) is widely used in mining application due to its helpful features despite all the financial costs. Therefore, designing and selection of a suitable belt for this system is very important for an accurate and long life operation. It is then required to understand and get familiar with the wear mechanism due to its destructive character and its highly occurrence in the belt and rubber during operation.

1.2 Project specifications

1.2.1 Project aim

The aim of performing this project is to investigate the effect of different factors such as test speed and normal load on the wear process of a rubber sample in mining applications. It is also to evaluate the wear mechanism on the rubber sample which is exposed to dry adhesive wear.

1.2.2 Timelines

This project will be presented in two parts; each for one semester. The first part of this project is more about the project theory such as the introduction about the project, literature review, methodology, resource and planning. This part was already started and finished by the end of May 2019. The second part of this project is more about experimental part including sample preparation, experimental set up, performing tests, data collection and data analysis. It is planned to be started from the Mid July 2019 and to be completed by the 7th November 2019. The Gantt chart presented below shows the tasks which are assigned to be performed in direction to complete this research project.

Table 1.1. Timelines of the project

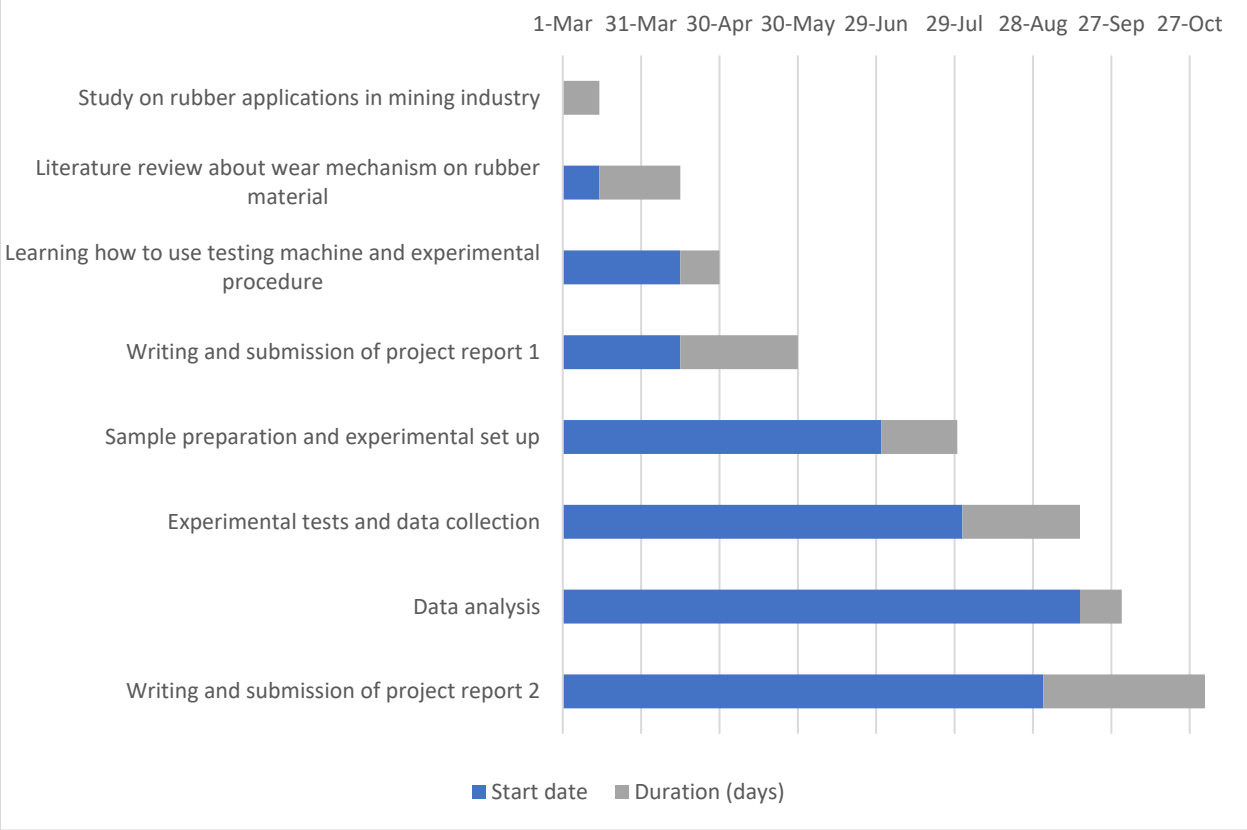

1.2.3 Risk assessment

Each experiment which is performed in the lab may be involved with some risks and dangers. The intensity of the risks is different and can be classified from low risk to high or extreme degree. To carry out a safe experiment, the regulations and instructions of the lab should be obeyed and safety induction must be performed before starting the experiment.

The lab which is located in Toowoomba campus of the university is treated like a cleanroom with controlled level of pressure and temperature. All students which enter the lab to conduct test are required to use Personal Protective Equipment (PPE). It includes all necessary wearing such as eye, head and earing protections, gloves, foot and leg protections to protect student's body in case of unforeseen dangers during the experiment.

Table 1.2 lists major risks and dangers which may happen during the experimental part of this project. The possibility, degree of intensity and the way which should be treated to manage the risks are given in this table.

Table 1.2. Risk assessments and treatments

List All Activities	Associated Risk(s)	Severity	Probability	Risk Score	Method(s) to treat the Risk
Learning how to use the lab instrument and adhesive test device	Damaging the test device parts	Medium	Low	Medium	follow up the instruction and manual of the device & using procedure given by the lab technician
	Damaging other instruments in the lab	Medium	Low	Medium	
Performing experimental tests	High speed rotation of wheel may damage fingers or hands	Critical	Low	High	Using Personal Protective Equipment (PPE)

	Sample may be broken in tiny parts and hit the face or eyes	Critical	Low	High	& Switch off the DSC device
General accidents	Fire in the lab Body injuries	Critical Critical	Low Low	High High	Turn off the lab electricity power, active the fire alarm & Using the first aid kit

1.2.4 Resource plan

As it was explained earlier, this project is about the investigation of wear mechanism on the rubber sample under adhesive wear. Therefore, the sample material for the experimental tests is rubber. Nitrile rubber was selected as the sample material. It is the most commonly used rubber material. This is due to Nitrile's compatibility with most environments as well as its lower cost compared to other rubber materials.

Nitrile rubber has good mechanical properties and high wear resistance relative to other elastomers. Unless they are specially compounded, nitrile is not resistant to weathering, sunlight and ozone. It is cheap and easy to access for performing experiments (Mykin, 2019).

The other required part is the testing machine for the adhesive wear test. This machine is available in the University of Southern Queensland. More details about this testing machine will be presented in Chapter 3.

1.3 Dissertation organization

First chapter of this dissertation was allocated to presenting a comprehensive detail about the wear process and mechanism which happens in different materials and particularly rubber material. Different types of wear were mentioned and more information about abrasive and adhesive wears was presented.

In the following chapters of this dissertation, a comprehensive literature review about abrasive and adhesive wears along with standard tests for this two wear types will be first presented in Chapter 2. In Chapter 3, explanations about the testing machine which was used for adhesive test under dry contact condition in this research work will be offered. The testing procedure will be also given in this Chapter.

Chapter 4 presents the results which was obtained during the experimental tests. It also gives discussions about the effects of different factors such as normal load, test speed and sliding distance on the wear parameters including volume loss, specific wear rate and friction coefficient. At the end, a conclusion about the findings of this research study will be presented in Chapter 5.

Chapter 2. Literature review

2.1 Introduction

As mentioned in the previous section, abrasive wear happens in the tools and devices with moving parts in the practical applications in industry which imposes cost and maintenance on the system. Therefore, many researchers attempted to investigate the wear mechanism and its effect on the system components. Some of the main research works in this category are presented in this section.

2.2 Wear mechanisms

There are different types of terms to categorize wear mechanisms. Figure 2.1 shows one of those classifications for wear mechanism. The main key words or wear and their sub-classes are summarized in this figure. As shown in Fig. 2.1, the wear mechanism depends of the contact type. Practically, there are different types of contact configuration such as normal or inclined compression, rolling and sliding. The rolling contact itself is divided to different types such as unidirectional, reciprocal and slip rolling. The sliding contact is also divided to unidirectional and reciprocal types. These contact classifications are all based on the motion of motion of contacting bodies.

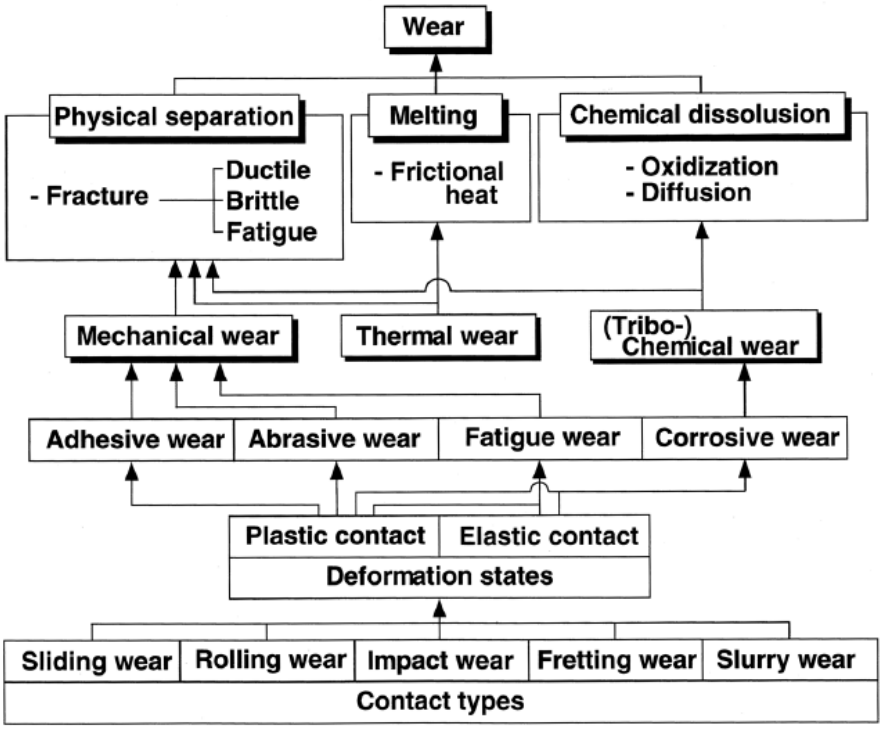

Figure 2.1 Classification of wear (Sasaki et al., 2013)

As a results of above mentioned contact types, wear is described as sliding wear, rolling wear, impact wear, fretting wear and slurry wear. Apart from the contact configuration, the severity of contact is also important for the wear mechanism. The most common and simplest ones are plastic contact and elastic contact. For this case, wear mechanism is categorized into four main types; adhesive wear, abrasive wear, fatigue wear and corrosion wear (Sasaki et al., 2013).

Out of these wear types, adhesive wear and abrasive wear are generated under plastic contact. When there is a plastic contact between similar materials, the interface of contact has an adhesive bonding strength. It is possible that fracture happens due to formation of strong adhesion at the contact surface. In this case, the resultant wear is adhesive wear, without description of fracture mode.

When there is a plastic contact between hard and sharp materials and the materials are relatively soft, the harder material gradually penetrate to the soft material. The fracture might be occurred with the method of micro cutting by the indented material. In this case, the abrasive wear happens between these two materials.

The other two types of wear mechanism, fatigue and corrosive wears, can be happened in both plastic and elastic contacts. Fatigue wear is it is clear by its name, happens after specific repeated cycles in the running in state contacts. In this case, when a surface failure is formed by fatigue, the occurred wear is fatigue wear.

In the case of corrosive wear, the tribochemical reaction at the contact surface is accelerated. If the material removal happens in one of the surfaces in contact under this condition, the wear mechanism happened is corrosive wear. The materials such as metals which are in contact with air, the tribochemical wear is called oxidative wear since the most corrosive elements in air is oxygen.

The material which is removed by wear in adhesive, abrasive or fatigue is usually governed by deformation and fracture in the contact region. The fracture modes in this case can be fatigue, brittle or ductile fracture. These kind of deformation and fracture are produced by the strains and stresses which are mechanically induced. Therefore, this type of wear is generally described as mechanical wear.

For the case of corrosive wear, the removed material which is governed by the growth of chemical reaction film or its solution on wear surface. The speed of chemical reactions depends significantly on different factors such as frictional deformation and heating. These parameters

lead to activation of reaction with a high progress and acceleration. The chemical wear or tribochemical wear is named for this category of wears.

In some cases, the generated heat during the friction of contact surfaces is too high which cases the material removal by surface melting. Furthermore, the thermal stress which is generated in a friction can lead to material removal by surface cracking. For the cases where the temperature difference or frictional heating is dominant, the wear is described as thermal wear.

Figure 3 shows the schematic images for the four wear modes of adhesive, abrasive, fatigue and corrosive wear. To analyse the wear, a comprehensive understanding of the wear type and affecting parameters on the wear is important.

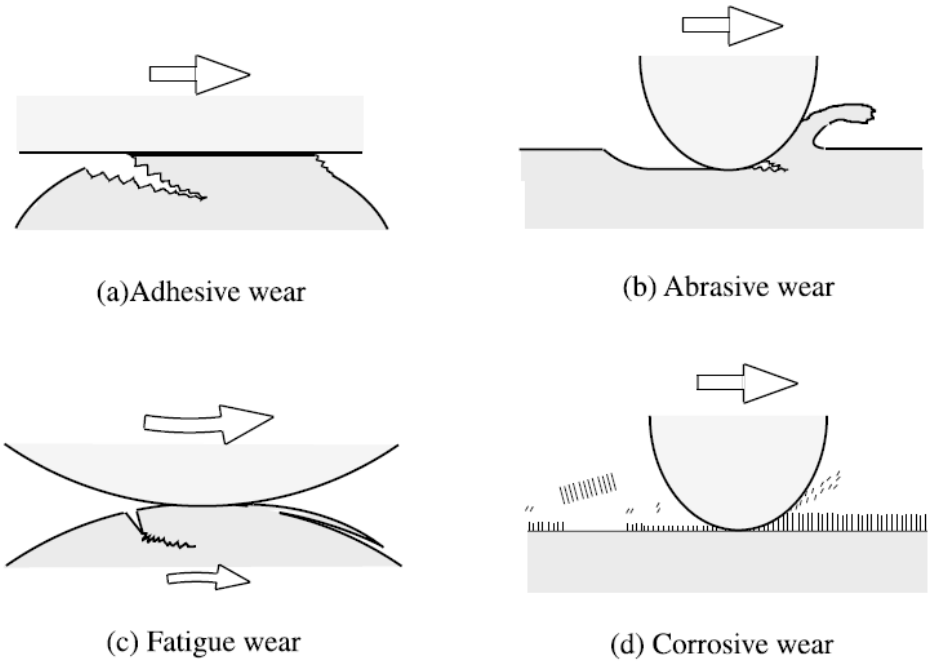

Figure 2.2. Schematics of different wear mechanisms (Sasaki et al., 2013)

For the case of belts and rubbers, the mechanism of wear is very complicated which depends on different parameters such as the magnitude of the normal load, texture and material of the rubber, temperature of the working environment and the speed of the belt. Some characteristics such as tearing and shredding are appeared in a worn rubber. In addition, some physical properties such as tensile strength, hardness and elongation are changed in a worn rubber (Tangudom et al., 2014).

The wear mode in the polymers are categorized into three parts: abrasion, adhesion and fatigue. With respect to this classification, three types of wear mechanism can be defined for rubbers; abrasive wear, fatigue wear and wear due to roll formation (Pal et al., 2009). Wear due to adhesive and abrasion are more important and more happens in polymers. A brief explanation about adhesive wear and abrasive wear are presented here.

2.2.1 Adhesive wear

With respect to the schematics of wear shown in Fig. 2.2 (a), an adhesive wear starts with a crack. For some plastic contact surfaces, the adhesive bonding strength is more than the relative sliding between the contact interface of two surfaces. It leads to creation of a large plastic deformation in the contact region under compression and shearing due to dislocation.

As a consequence of such a large deformation in the contact area, a crack is generated and is progressed in the combined fracture mode of tensile and shearing. As the crack advances and reaches the contact interface, a wear particle is produced and adhesive transfer is completed. Therefore, the adhesive wear is a type of wear which happens if the adhesive bonding strength at the contact interface is more than the relative sliding.

From another point of view, adhesive wear is defined as a type of wear which is generated by sliding one solid surface along another surface. When two surfaces are loaded against each other, the whole contact load is carried only by the very small area of contacts. The real contact pressure over the asperity is very high, leading to adhesion between them. The adhesive junction can be broken if one of the surfaces slides against the other. As sliding continues, fresh junctions will form and rupture in succession. The adhesive wear can be minimized by using lubricants or by the application of hard coating with a low coefficient of friction (Majumdar and Manna, 2015).

Figure 2.3 shows the schematic of the material removal in adhesive wear. A wear particle is produced for the time on which a bond junction is broken. The material removal usually happens from the weaker material. In addition to the applied load and material resistance, the roughness of contacting surfaces is also important in adhesion wear mechanism. The particles which are removed from one surface may stick to another surface. They can be deported from the bearing coupling or be kept in the bearing joint which later on cause abrasive phenomena.

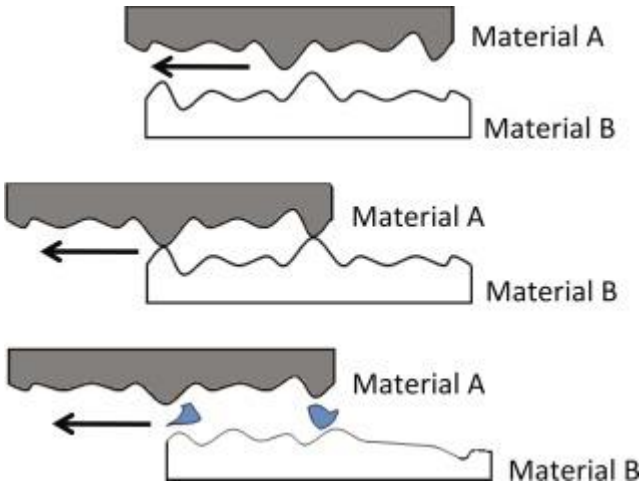

Figure 2.3 Material removal in adhesive wear (Tanzi et al., 2019)

Figure 2.4 shows the adhesive wear mode and completion process for the thin flake-like wear particle in part (a) and a wedge-like wear particle in part (b). As shown in this figure, when a tangential shear occurs with compression at the contact interface of strong adhesive bonding, different slips are formed along the slip planes in the contact region et the end of completion.

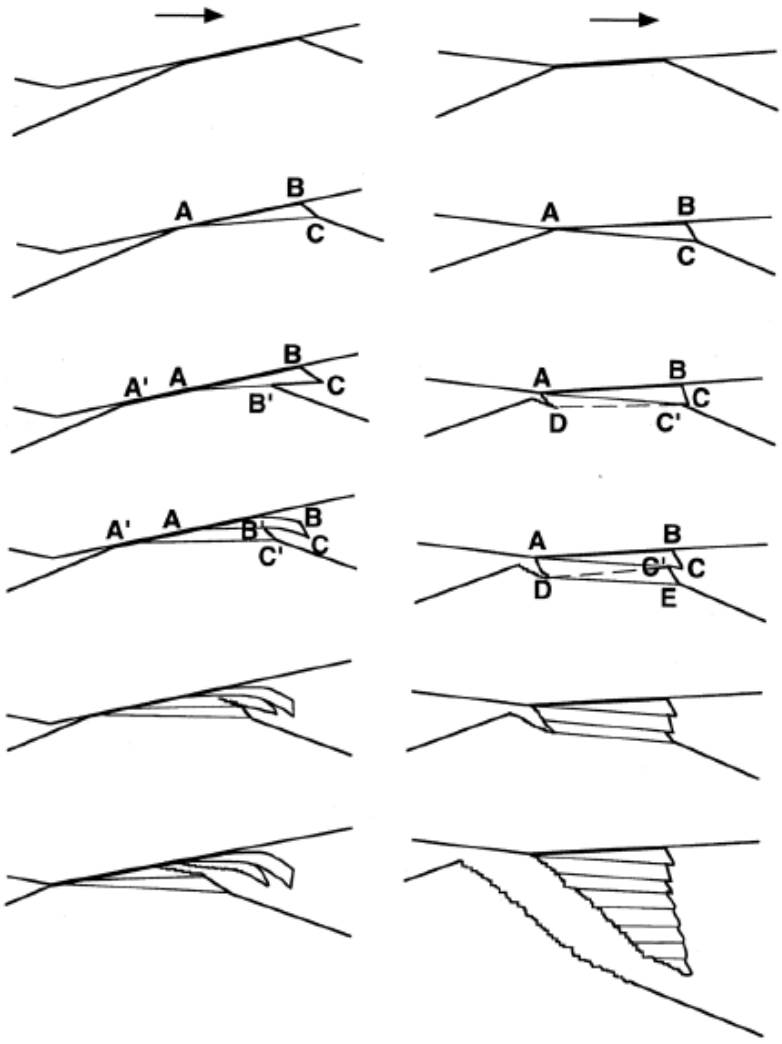

Figure 2.4. Adhesive wear process, (a) thin flake-like wear particle (b) wedge-like wear particle (Kayaba and Kato, 1981)

As a result of these generated slips, flake-like shear tongues are formed as shown in Fig. 2.4 (a). these slips are then followed by a crack initiation which makes progress in the combined fracture

mode of tensile and shear in the leading region of the contact. If the plastic deformation is high enough in the contact region, it leads to formation of a wedge-like shape as shown in Fig. 2.4 (b). It is then followed by crack initiation which advances in the combined fracture mode of tensile and shear but this time in the trailing region of the contact.

Fracture analysis of the generated wear particles shown in Fig. 2.4 indicates the fracture mode of compression and shear for the larger part of the fracture surface of the flake-like wear particle. It also indicates a tensile and shear fracture mode for all parts of the fracture surface of the wedge-like wear particle. The fact is that both wear modes which create the flake-like and wedge-like wear particles are of basic ones in adhesive wear.

As stated by Sasada (1984), transfer and re-transfer from one sliding surface to another surface happens in many cases in the adhesive wear process. As a result, the formed wear particles which are sometimes relatively large in size are a composition of two surfaces. This is another basic part of the adhesive wear mechanism.

In the successive process of repeated sliding, the generated wear particles may leave the contact interface as free particles or stay on either surface to scratch the counterface. Even if the contact surfaces are flat with similar materials and the contact interface is first parallel to the sliding direction, the interface rotates and becomes inclined and wavy as a result of the combined effect of normal and tangential forces in sliding (Cocks, 1962).

Adhesive wear is affected by different variables. Some of these variables are difficult or impossible to measure. As a result, no unique equation can be suggested to estimate the maximum volume of wear. Based on the adhesive mechanism, Archard (1980) suggested an

equation for calculation of adhesive wear which is called Archard model. This equation is written as:

$$w = k\frac{Ld}{H} \quad (1)$$

In this equation, w is the volume of the wear, L is the applied load, d is the sliding distance and H is the hardness of the softer material. The wear coefficient k is a dimensionless constant. As a first approximation, this coefficient can be considered as the probability that a micro-junction is produced by a wear particle.

Measured values of K are frequently small and range from 10^{-8} to 10^{-3}. The 10^{-8} is related to the incompatible metals rubbing against each other with good lubrication. The value of 10^{-3} is for clean surfaces with no lubricant of like metals. The small values of K along with the original interpretation of K propose a probabilistic interpretation of the wear coefficient. It actually describes the fraction of the actual contact surface which is removed by the wear process. It can also describe the possibility that any given individual friction contact event reaches to the maximum possible with the removal of a wear particle.

It should be noted that if the sliding distance is as a result of sliding at constant velocity U, the sliding distance d is calculated by $d = Ut$, where t is the sliding time.

There are two limitations for using Archard model. The first one is that the wear is not always inversely proportional to hardness. However, it depends on the way that the hardness is formed in the microstructure of the material. The second limitation is that the theoretical wear coefficient is always very far from actual results (Affatato and Brando, 2013).

2.2.2 Abrasive wear

One type of wear happens due to friction between sliding particles and rigid materials. For the case of a conveyor belt system, it occurs between the pulleys and belt in one hand and the belt and raw materials which are carried on the other hand. The main factors which generate this kind of wear are longitudinal stretches and micro-cutting due to sliding materials and sharp tips of tiny particles of transported materials on the belt (Muhr and Roberts, 1992).

Generally, there are two types of abrasive wear: two body abrasion and three body abrasion. A combination of these two types can also exist. The part which experiences the most wear is denoted as the first body. The second body exerts force by relative motion, either directly or indirectly and leads to the wear of the first body. A third body is introduced to the first and second bodies by an external source or formation of particles during the wear process. The third body can include different materials such as debris, lubricants or entrained particles (Gates, 1998).

Figure 2.5 shows a schematic of two and three body abrasion wear. As shown in Fig. 2.5 (a) of this figure, in two body abrasion, the wear occurs by sliding the surface of a first body on the surface of the second body which has an opposite motion. It is seen in Fig. 2.5 (b) that some particles are trapped between the surface of the first body and the surface of the second body. These very small particles are considered as the third body and that's why this kind of wear is kind three body abrasion wear. These particles are free in motion between two other surfaces in rolling or sliding.

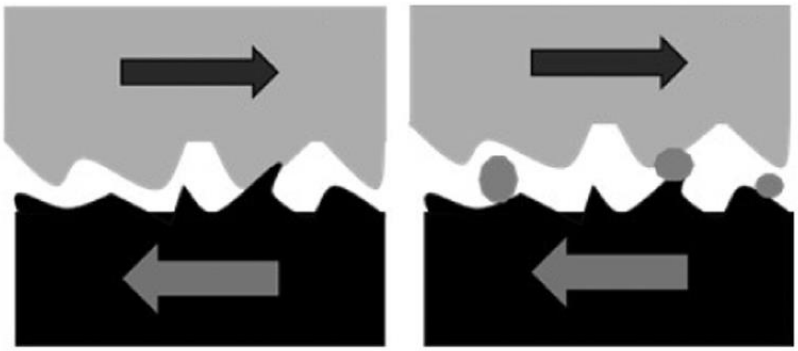

(a) (b)

Figure 2.5. Abrasive wear: (a) two body, (b) three body (Hakami et al., 2017)

In general, two body abrasion happens in small scale testing machine such as tribological tests in lab. However, three body abrasion mostly occurs in practical applications and in reality such as abrasive wear which happens in a conveyor belt system in mining or other kind of industrial applications (Molnar et al., 2014).

The abrasion can be also classified in high stress and low stress abrasions depending on the level of stress during abrasive wear. The low stress abrasion is also called scratching abrasion and the high stress abrasion is also named as grinding or gouging abrasion. The high stress abrasion occurs by the contact of abrasive particles with sharp edges. This can be created by breaking the particles in contact area under a high contact stress. The low stress abrasion happens during a light load which causes the abrasive particles impinge on and move across the wear surface. It leads to scratch and cut the material on a very small scale (Liu et al.).

Abrasions which is created by sand paper for example, is categorized as a high stress abrasion as it remains sharp during the wearing process. The process of ISO 4649 test is a sample of this kind of high stress abrasion. High and low stress abrasions are usually defined by the value of the

normal and stress and the contacting forces which exists between the abrasive particles and the abraded surfaces (Budinski, 2011).

One of the main problems which happen in the systems with moving parts is the abrasive wear which causes failure in some cases. Tiny particles which are created during the working process of system enter between the sliding components. As a result, abrasion wear occurs on the system gradually during the time. It is the most costly form of wear in practical applications in industry. As a result, to have the best optimized system with the highest working life, knowing the mechanism of abrasive wear is very important (Mukhopadhyay, 2016).

During the abrasion wear of a rubber, a series of ridges are formed on the surface of rubber in contact with the second or the third body. The direction of ridges is first perpendicular to the sliding direction and then deformed. Figure 2.6 shows the abrasion pattern of a rubber sample in a laboratory test. The pattern directions can be seen that is almost normal to the moving direction as indicated in this figure. The effects of abrasion on a worn surface appear as different shapes and types such as scratches, gouges and scoring marks.

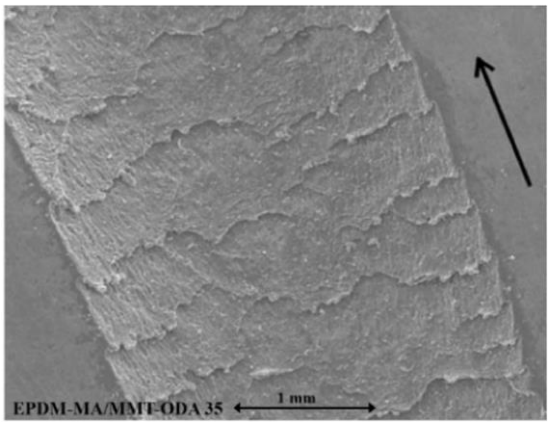

Figure 2.6. Pattern for abrasion in a sample test rubber (Hakami et al., 2017)

One of the important tests to find the nature and pattern of the abrasive wear of rubbers was proposed by Schallamach (1952). A needle was used in this test to scratch the surface of the rubber under different values of normal loading and sliding velocity. As shown in Fig. 2.7, the surface of rubber was loaded with a series of discontinued needle traces. The material loss in the rubber surface is very little by the scratch of a needle, but as seen in Fig. 2.7, the surface damage is significant.

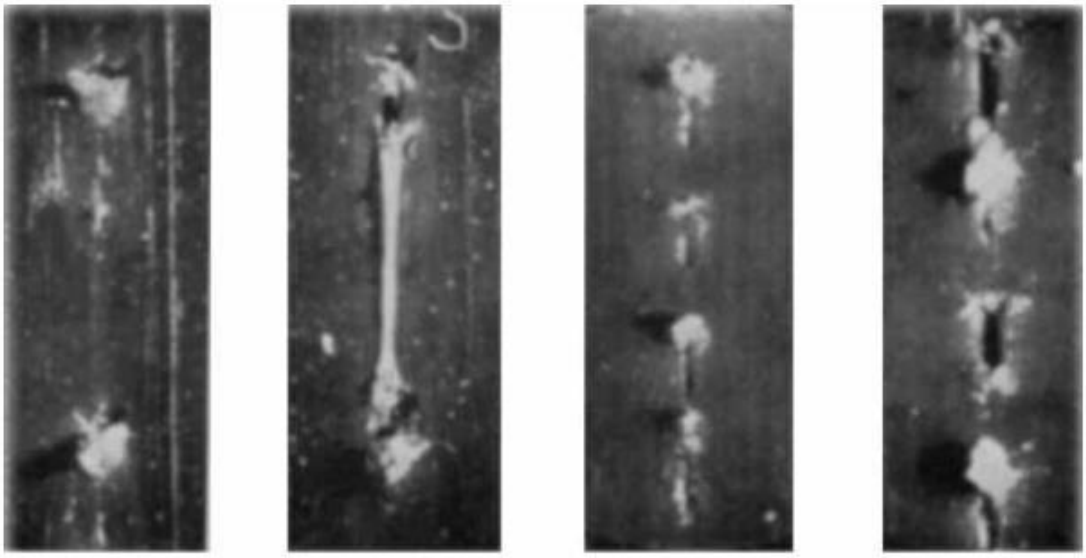

Figure 2.7 Needle trace on the rubber surface generated by different normal load (Wu, 2017)

Figure 2.8 shows a schematic of the groove formation on the rubber surface by the needle. This picture clearly demonstrates the stress concentration and strain distribution around the tip of the needle on the surface of the rubber. The curves are originally placed in equal distance from each other, perpendicular to the sliding direction before deformation happens. After imposing the needle, the lines are deformed by the needle tip which shows the strain distribution and stress concentration around the needle. The largest stress initiates at the front of needle but it is still less than the rubber adherence and therefore, no failure occurs. But the rubber tears at the

location where it loses the with the needle (Wu, 2017). Instead of using just a single point of contact and with the purpose to have a measurable amount abrasion loss, researchers use a multiple points of contact with sharp asperities such as abrasion of rubber by sliding on a silicon carbide abrasive paper.

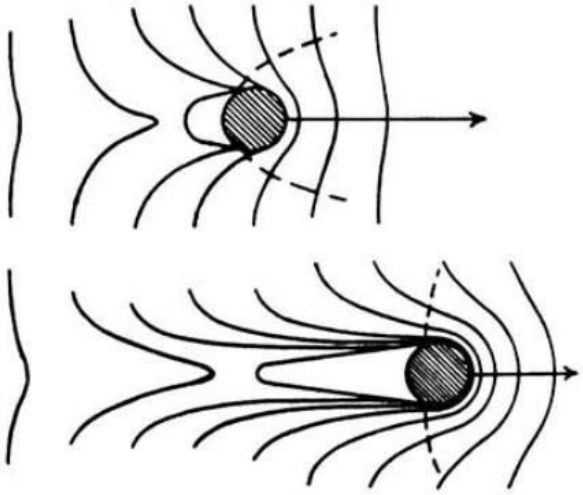

Figure 2.8. A schematic of stress concentration and strain distribution of the surface of the rubber around the tip of the needle (Wu, 2017)

2.3 Standard tests for wear of rubber

There are different standard test methods presented by standard organizations to measure the resistance of materials against abrasive wear. International Organization for Standardization and the American Society for Testing and Materials are two main organizations which present standard test methods for adhesion and abrasion in materials.

2.3.1 Adhesive wear

One of the standard test to measure the adhesive strength pf rubbers is ASTM D429. This test determines the adhesion of rubber to rigid metal substrates. There are different methods for this

test from method A to method H. This standard test can be used for different applications such as vehicle engine mounts, vehicle suspension bushings, rubber-coated metal parts and rubber lined tanks and containers. Almost all tests include orthogonal tensile strength or compressive strength of the adhesion interface. However, few tests are performed with the purpose of measurement the shear strength of that adhesion interface (testresources, 2018).

As mentioned above, this standard test has different methods from A to H. The method A, for example, is to determine the static adhesion strength of rubber to metal. It measures the adhesion values for the cases where the users believe a design is more reflective of an actual product. The sample in this case is used for testing the effectiveness of different processing techniques and different adhesive systems.

The method B of ASTM D429 test is defined to measure the adhesive strength of rubber to metal bonding. This test is performed by a 90-degree peel strip. The results are obtained by measuring the force which is required to separate a rubber from a metal surface. The data test which is obtained in this test shows the strength of adhesion along a line across the width of the rubber strip. This rubber strip is separated from a metal plate at a 90-degree angle.

Test Method C of ASTM D429 measures the adhesive strength of rubber to metal bonding agents for the case of applied to conical or cone-shaped samples. This test includes both tensile and shear forces in the rubber specimen material. This is not a dynamic test but it may be used for vibratory or vibration applications. Figure 2.9 shows a schematic of this standard test. The information about other test methods from D to H can be found in testresources (2018).

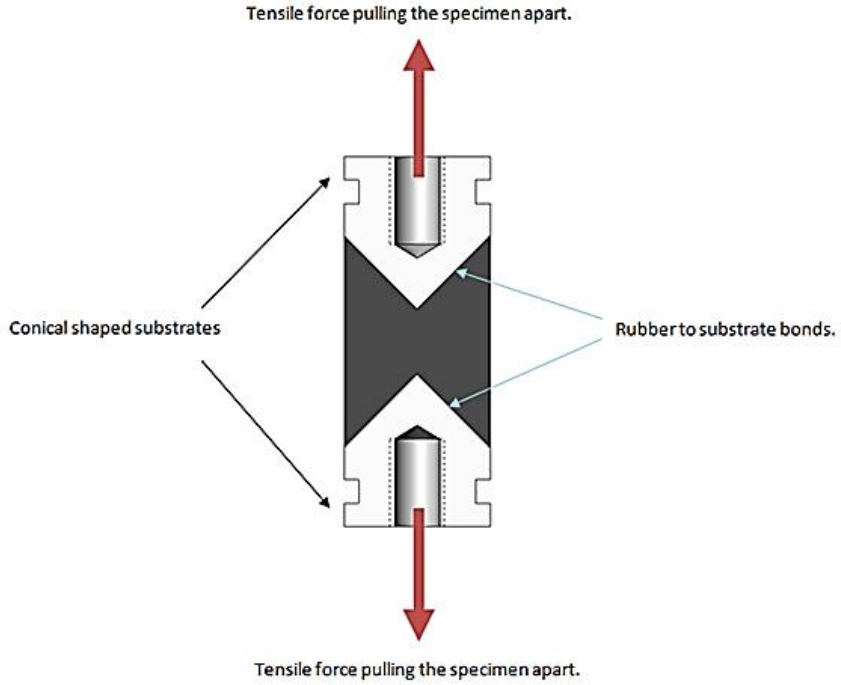

Figure 2.9. ASTM D429 method C (Applerubber, 2019)

ASTM D413 is another standard tests for adhesive wear of rubbers. It helps determine the quality of a product. This quality is obtained by measuring the force per unit width which is required to separate a rubber layer from a flexible sublayer like fabric, fiber, wire or sheet metal. The ASTM D413 test is used when the adhered surfaces are almost plane or uniformly circular. These kinds of surfaces cab be found in belting, hose, tire carcasses or rubber-covered sheet metal.

In the ASTM D413 test, an adhesion test includes a measured force which is enough to strip from the specimen at a measured rate and a layer of moderate thickness with separation (rupture, tearing) at the adhered surfaces. Adhesion is reported as the average force which is required for separation at a definite rate or is expressed as the average rate of separation which is caused by

a known or specified force. Similar to the ASTM D429 test, the ASTM D413 test is defined by different methods which are A, B and C. Figure 2.10 shows a schematic of the ASTM D413 test.

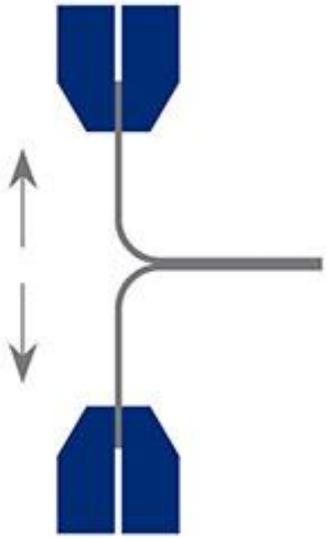

Figure 2.10. ASTM D413 test (Mecmesin, 2018)

The ASTM G77 is another standard test for the adhesive wear. This test is to determine the resistance of materials to metal to metal sliding wear. As shown in Fig. 2.11, it uses a block on ring testing machine to rank pairs of materials based on their sliding wear compatibility properties. This test replicates adhesive of a metal to metal wear. The results of this test are presented for the removed material as the volume loss in cubic millimetres for both the block and the ring. It is clear that the materials with higher wear resistance have lower volume loss. Friction coefficients may also be established during this test.

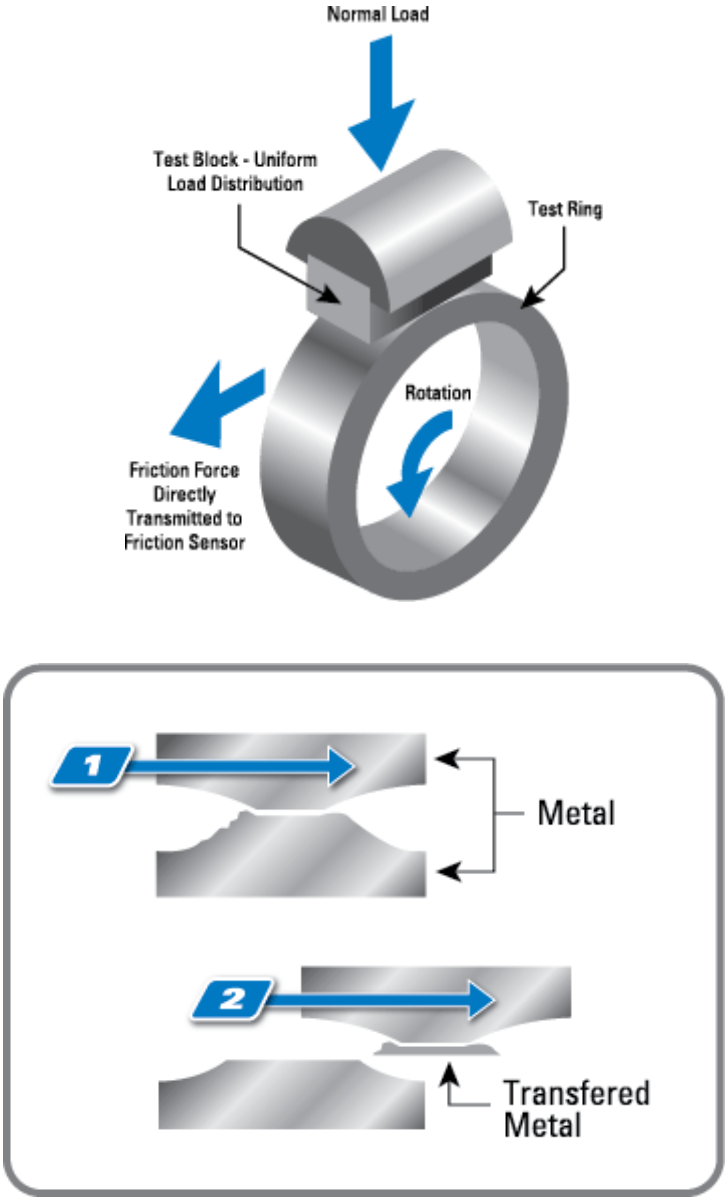

Figure 2.11. ASTM G77 standard test for adhesive wear (coatings, 2019)

This test is performed based on a 3000-meter slide length. The applied load is fixed in a normal direction compressive load with a magnitude of 300 ponds force. The mineral oil lubricant is used in this test. The revolution of rotating ring test is 30000 revolutions. The tested material can be rubber instead of metal in this testing method.

2.3.2 Abrasive wear

The standard tests for abrasive wear are ISO 4649, ASTM G65 and ASTM G 174. The ISO 4649 is a test for two body abrasion and includes two methods for estimation the rubber resistance to abrasion using a rotating cylindrical drum. These methods which are categorized in A and B, determine the volume loss of rubber by abrasive action of rubbing a sample over an abrasive sheet with a specified grade. Method A is used for a non-rotating sample and method B is used for a rotating sample test. The results for each method can be presented as a relative volume loss or an abrasion resistance index.

The performed tests based on ISO 4649 are all comparative due to some affecting parameters on the testing procedure which lead to variations in the absolute values of abrasion loss. These factors include the grade of abrasive sheet, the type of adhesive used for the producing the sheet, contamination and wear caused by previous testing.

A different test is also performed with a reference compound so that the results can be presented either as a relative volume loss compared to a calibrated abrasive sheet or as an abrasion resistance index compared to a reference compound. These tests are useful for different purposes including quality control, comparative tests and research and development work. Figure 2.12 shows a schematic diagram of ISO 4649 testing machine.

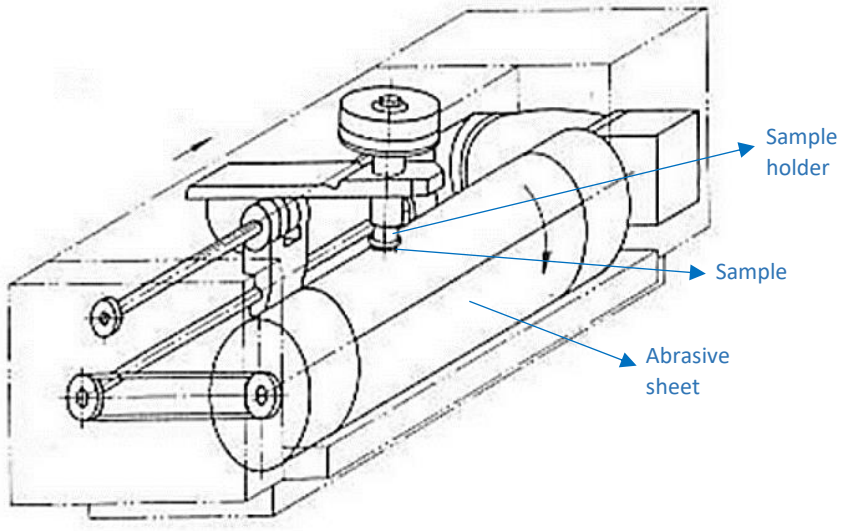

Figure 2.12. Schematic diagram of the ISO 4649 test device

Another standard test to measure abrasion wear is the ASTM G65 standard test method. This method is used for three body abrasion and the third body is usually sand. This is a low stress abrasion standardized test (Doering et al., 2011). In ASTM G65 standard test, a test specimen is loaded against a rotating rubber wheel and get in contact with abrasive particles, either dry or wet sand. An abrasion wear testing machine based on ASTM G65 standard dry test is shown in Fig. 2.13. Part (a) is a picture of testing machine and part (b) is a schematic of the interior side of this machine showing its different components to perform a dry wear test. The dimension of specimen should be 12.7 × 25 × 76 mm.

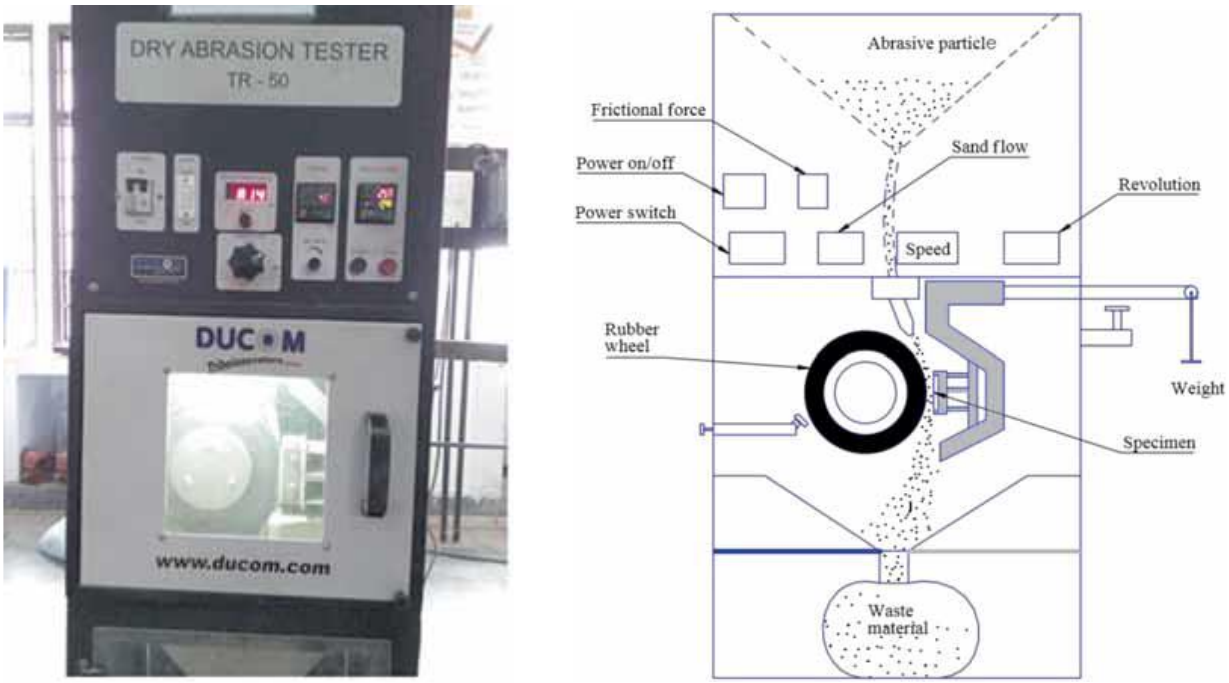

Figure 2.13. Abrasion wear test machine TR-50. (a) photograph of the machine, (b) schematic of the interior components (Singh, 2016)

As shown in Fig. 2.13 (b), the specimen is pressed to the rotating rubber wheel. The value of pressing load and the rotating speed of rubber wheel is adjustable by some button in the panel shown in Fig. 2.13 (a). The specimen has a sliding motion along the rotating wheel axis during the test. The testing process in continued by a controlled amount of the third body abrasive particles coming from top side which flows between the rubber wheel and the test specimen. The specimen is weighted before and after the test to record the loss in its mass. But due to a high difference in material densities, the abrasion is determined as per the loss in volume based on the following equation (Singh and Siddhartha, 2015):

$$W_s = \frac{\Delta m}{\rho L F_n} \tag{2}$$

In this equation, W_s is the specific wear rate, Δm is the mass loss in the specimen during the test, ρ is the density of composite, L is the sliding distance of the specimen along the rotating wheel and F_n is the normal pressing load. The specific wear rate is then actually the loss in the volume of the specimen ($\Delta m/\rho$) per unit sliding distance (L) per unit pressing normal load (F_n).

The ASTM G 174 which is shown in Fig. 2.14 is developed to measure the wear resistance of materials against two body abrasion. In this test, the specimen is fixed in its place and a loop of abrasive which moves around three rollers and shaft, applies force on the specimen. According to the procedure of this standard test, the specimen dimension should not exceed over 3 × 7.6 × 32 mm. The loop is continuous and contains 30 µm aluminium oxide finishing tape to abrade the specimen (Budinski and Budinski, 2017).

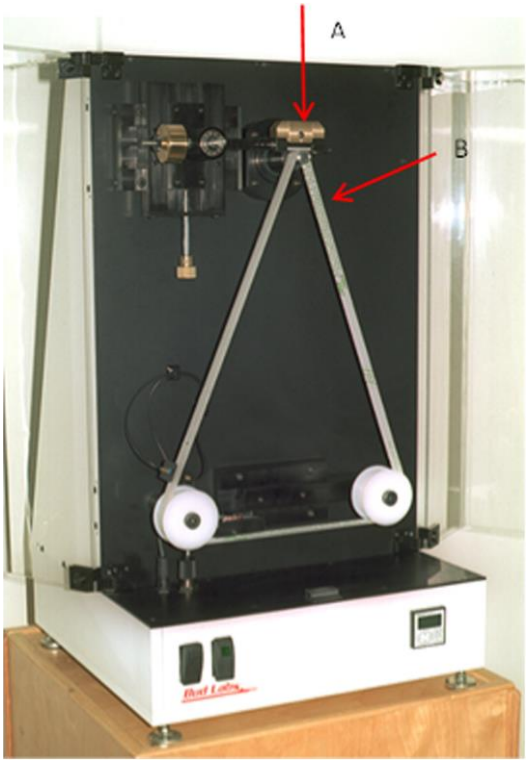

Figure 2.14. ASTM G 174 abrasion test; A is the specimen and B is the moving strip (Budinski and Budinski, 2017)

2.4 Laboratory tribo-test machine

Up until now, different laboratory tribo-test machines have been designed and fabricated based on the mentioned standard tests in the previous section. These machines are developed to investigate the tribological properties of different materials such as rubber based on using individual technique.

The most common methods for this investigation are the block-on-disc method (BOD) based on ASTM G99, the block-on-ring (BOR) technique based on ASTM G77-98, the dry sand rubber wheel (DSRW) based on ASTM G 65, the wet sand rubber wheel (WSRW), according to the ASTM G105, and sand/steel wheel (SSW) test in wet/dry conditions based on the ASTM B 611.

Figure 2.15 shows the different testing machines used for the most common techniques for tribological experiments. These machines are used for both adhesive and abrasive wear tests. Figure 2.15 (a) shows the testing machine based on the block on disk (BOD) technique. Figure 2.15 (b) shows a schematic for the machine based on the block-on-ring (BOR) method. And Fig. 2.15 (c) indicates the apparatus for the dry sand rubber wheel (DSRW), the wet sand rubber wheel (WSRW) and sand/steel wheel (SSW) methods. The contact mechanism of the tested materials with the counterface is the main differences between these testing methods. The possible contact mechanisms include area, line or point contact.

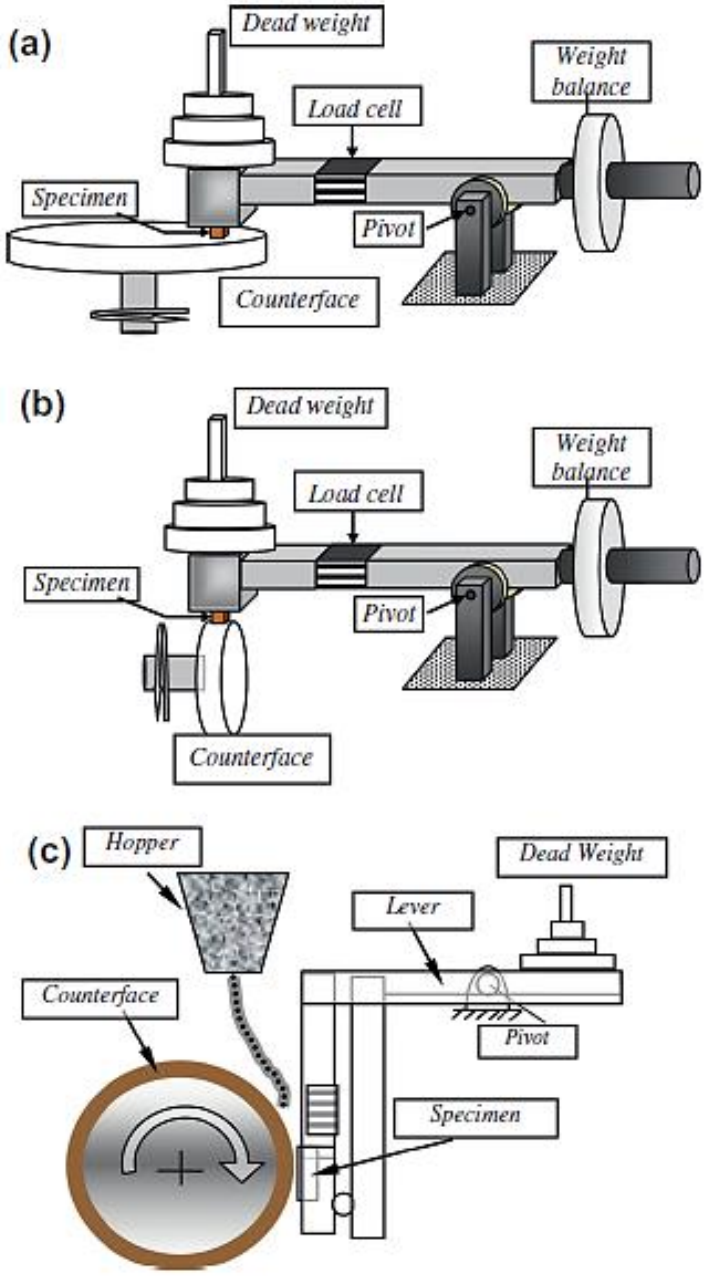

Figure 2.15. Schematic drawing showing the most common configurations of tribological machine for adhesive and abrasive testing. (a) block on disc (BOD), (b) block on ring (BOR) and (c) dry sand rubber wheel (DSRW), (Yousif, 2013)

A new testing machine which combines all the above techniques in one device was designed and fabricated by Yousif (2013). Figure 2.16 shows this apparatus in the University of Southern Queensland. This is a multi-functional machine which can be used for two testing techniques

including the block-on-disk and the block-on-ring techniques with different operating conditions as dry or wet. This machine was used for the experiments in this research study. More explanations about this apparatus are presented in the Chapter 3.

Figure2.16. Multi-functional tribo-test machine (Alshammari et al., 2018)

2.5 Wear process

The first person who investigated the failure of rubber by using a sharp needle passing over the surface of rubber was Schallamach (1952). In this work, the needle was used to make scratch on the rubber surface under controlled conditions. The purpose was to study the nature and pattern of the abrasive wear on rubber. The presented pattern of abrasive wear and the following mechanical failure which happens and produce periodic surface pattern was then named Schallamach waves.

Hakami et al., (2017) investigated the rate and mechanicm of wear of rubber together with their associated factors according the information which are presented in the literature. They claimed that the most important types of wear are abrasion, fatigue and roll formation which get affected by the amount of loads, sliding velocity, friction and hardness of abraded material. They also made a correattion for those effective factors on the wear of rubber. They concluded that the adheision wear makes roll for the case of smooth surface when tear strength of rubber is not high.

Li et al. (2019) performed a simulation with an integrated approach to investigate the friction and wear of tire tread rubber. They considered different factors which affect the friction and wear of this type of rubber. One of them was the local nonlinear constitutive equation for friction and wear in the contact interface. The other parameter was the solving strategies such as wear increment optimization and worn mesh update. They proposed a modified friction test scheme of rubber wheels together with the numerical validation, which considerabely imroved the distribution uniformities of the contact pressure and sliding velocity.

Khafidh et al. (2019) investigated the wear processes of short-cut aramid fiber reinforced elastomers as a function of sliding distance and their relation to friction. The aim was to analayze the way that fiber reduces the propagation of cracks in order to decrease the wear. They considered two different types of reinforcing systems, including the elastomers reinforced by solely short-cut aramid fibers and elastomers reinforced by short-cut aramid fibers and silica. The obtained results showed that the friction behavior of elastomeric composites is highly affected by the wearing process. In addition, they found that friction coefficinet decreases with the presence of fibers on the wear surface.

2.6 Adhesive wear

Gåård et al. (2010) conducted different sliding tests under dry contact condition to investigate the effects of temperature of the adhesive wear. The experiments were performed at different sliding velocities and different surface temperatures due to frictional heating. The obtained results showed that there is a significant effect of temperature on adhesion and that the increasing temperature results in a higher tendency for start of an intense adhesive wear. They found that the temperature enhancement increases the adhesive force between contact surfaces.

Laux (2016) performed a research study research is to obtain a thorough understanding of adhesive wear phenomena in polyaryletherketone (PAEK) polymers. The purpose was to find a correlation between the observed surface damage and friction response. They found the formation of transfer films which look like a unidirectional drawing process. The results showed that these transfer films play an important role on describing the friction and temperature responses of the PEEK wear interface.

Aghababaei et al. (2016) used an atomistic simulation with model interatomic potentials to investigate the transition in the asperity wear mechanism. They tried to propose an analytical model to predict this transition. The effects of critical length scale on the adhesive wear behavior was also studied. They found a transition in the asperity wear mechanism when contact junctions fall below a critical length scale. It was revealed that predictions of two distinct adhesive wear mechanisms can be combined into a unified framework.

In another related work, Aghababaei et al. (2017) studied the long-standing microscopic origins of material detachment from solids surface at the highest basic level such as wear debris particles. They aimed to estimate the volume of the detached particle using frictional work, instead of using empirical factors. The simulation results showed that the asperity junction size significantly affects the debris volume and existence of a correlation between the wear volume and the real contact area. They found however, there is no correlation between the debris volume and the applied normal force at the level of debris. They also realized that the junction size controls the tangential force and sliding distance.

Milanese et al. (2018b) adopted an approach to investigate the surface roughness progress under adhesive wear processes. The focus of their research was for the case on which the material loss is mainly due to transfer of particles from one body to another. The used a two-dimensional simulation with periodic boundary conditions along the horizontal direction to allow for continuous sliding at constant velocity of the top surface over the bottom one. The simulation results indicated that after the running-in condition, the generated debris particles can significantly disturb the wear process increasing against the roughness of the mating surfaces. They observed that the increase of surface roughness happens by removal of material from the opposing surfaces when the particle is approximately round.

In another research work, Milanese et al. (2018a) developed atomistic simulations in order to obtain significant understandings of the physics of surface roughness evolution during adhesive wear processes. They stated that the progress of the surface morphology is divided in two different phases: running-in and long-term sliding. In the phase of running-in sliding, two surfaces come into contact at the asperity level. They found that the asperities deform plastically if the

junction which is formed by two colliding asperities is smaller than this critical length. The asperities will break if the otherwise condition exists. About the progress of surface roughness, they observed that the surfaces will smooth continuously until they weld together if the junction is small. For the case the junction size is large enough, a debris particle is formed by fracture which creates roughness.

Karsli et al. (2018) investigated the effects of addition of coupling agent on the adhesive wear as well as thermal and morphological properties of glass fiber-reinforced polyamide PA6,6 composites. They used Phenylene-bis-oxazoline (PBO) as the coupling agent for glass fiber and PA6,6 to increase the interfacial adhesion between them. Different tests were performed based on the different levels for the weight percentage of coupling agent. The analysis of the experimental data showed that an addition of 2% PBO will increase the fiber–matrix adhesion. It also improves the adhesive wear resistance of glass fiber-reinforced PA6,6 matrix composites.

Fereidouni et al. (2019) performed an experimental investigation for the assessment of adhesive wear subjected to variable loading. They aimed to check the possibility of use of the Miner's rule to variable loading and estimation of the Miner's rule constant. The pin-on-disk technique with variable loading was selected for this experiment. They found that the cumulative power dissipation and entropy remain almost constant and independent of the loading sequence. They also offered an accurate method for estimation of wear under variable loading.

Frérot et al. (2019) investigated the effects of plastic deformation on the macro-scale wear response and the formation process of crack as a result of adhesive wear in a rough elastic-plastic contact. They used a classical J_2 plasticity approach and a saturation plasticity model for their

investigations. The obtained results revealed that the plastic residual deformations in the J_2 model intensify the tensile stresses of surface which results in a higher possibility of crack formation for contacts. For the case when the material is more ductile, this effects showed to be more intensive.

Brink and Molinari (2019) investigated the formation of wear particle for sliding interfaces in dry contact with full and reduced adhesion. They suggested a mechanism map based on the material properties and local geometry. This mechanism was validated by using quasi-two-dimensional and three-dimensional molecular dynamics and finite-element simulations on a silicon like model material. They found that colliding surface asperities can either deform plastically and generates wear debris particles or slip along the contact junction surface without significant damage.

2.7 Abrasive wear

Molnar et al., (2018) studied the effects of two and three body abrasion on rubber belts used in conveyor belt systems. They used two standard tests with the name of ISO 4649 and ASTM G 65 for their investigations. They performed tests with the attention to the high temperature working conditions such as the cases of steel industry and transported goods. As a result, they modified the standard tests to be suitable for temperatures up to 200 °C nad named it ISO 4649M.

Figure 2.17 (a) shows a schematic of the modified test of ISO 4649. The tester was equiped with a heating collar around the sample so that it can be heated up to desired temperature. Another change in this test compared to the standard ISO 4649 was the overlap size for the sample. In ISO

4649M, a 3 mm overlap was used for the sample instead of 2 mm, to insert the thermocouple into the sample.

They also modified the standard test of ASTM G65. As shown in Fig. 2.17 (b), the modified tester was equipped with two heating system in order to heat up the sample and abrasive individually. The modified test was to simulate the condition where be belt is heated up with hot transported goods in practical applications. The ISO 4649 standard test representatives a two body abrasion while ASTM G65 for the three body abrasion test.

Their investigations presented a view of the wear loss and wear mechanism based on the collected information. They conculded that the ASTM G65 performs better for simulation of wear which is caused by the loose goods which rools freely on the belt, whereas the ISO 4649 test is more suitable for explaining the scraper belt contact.

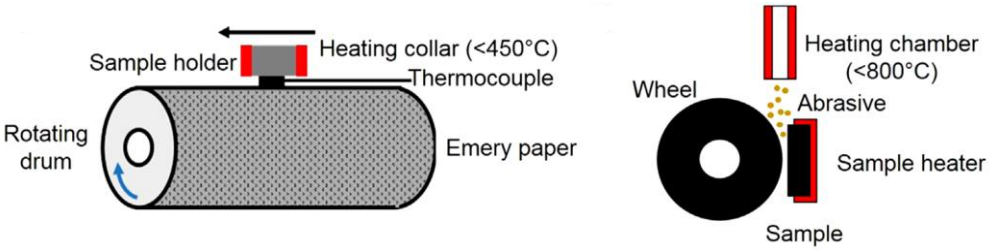

(a) (b)

Figure 2.17. Schematic of the modified tests, (a) ISO 4649 and (b) ASTM G65 (Molnar et al., 2018)

Holmberg et al. (2017) presented a calculation on the usage of global energy which are caused by friction and wear in the mineral mining industry. They included the effect of wear in their calculations to indicate its significant tribological and economical influences in mining industry. In this calculation work, they analyzed the wear effects on the several equipments used for different purposes in mining such as extraction, underground and mineral processing. They suggested some potential works to decrease the wear effects in mining. These include development and use of new materials with higher strength and hardness properties, improved surface coating and new lubricants or lubricant additives.

Huang et al. (2018) developed a rotary tribo-meter machine to reproduce the abrasive wear of reinforced rubber materials for tire. The innovative device was able to perform accelerated, quantitative friction and wear test which simulated to the real condition of kinematics and dynamics of the contact. The focus was on the significant effect of wear debris collected in the contact zone on the measured wear rate. The measure this effect, the amount of this type of wear was varied by changing the frequency at which debris are diminished. They found that the wear rate decreases as the wear debris increases in the contact zone.

Shen et al. (2016) investigated the features of the two body abrasion wear for a particular rubber type (nitrile butadiene rubber or NBR) and also the influence of abrasive size on the abrasion wear. They performed reciprocating abrasive wear tests on a NBR pin against an abrasive sand paper with the roughness of 2.5 μm for small size to 200 μm for the large size. In this investigation, the compared the values of different friction coefficients and the wear rates. They concluded that the size of abrasives affects significantly on the wear mechanical and tribological properties of NBR. They also found by decreasing the abrasive size, that the wear mechanism

changes from abrasive wear to adhesive wear. For the small abrasives, the coefficient of friction decreases as the abrasive size increases. However, this pattern is reversed for the large abrasives.

Stachowiak et al. (2016) studied the effects of particle angularity on the tribo-electrochemical behavior of steel material under the condition of low stress with three body abrasion and corrosions. They used particles with different angularity and entered them to the interface between the specimen tests and rotating drum based on the ASTM G65 test and changed the amount of current with time. They proposed an empirical correlation using the linear relationship between the load and speed and the average current. The experimental results showed that the depassivation efficiency of the improves by increasing their angularity.

Holmberg and Erdemir (2019) presented a short overview on the effects of friction and wear losses on the global energy efficiency. They claim that friction consumes over 20% of the total energy which exists in the world and over 35% of the energy used for transportation is consumed to overcome the friction. Based on their investigations, improving the systems with new materials, lubricants and design can reduce the loss of energy by friction and wear up to 40%. This saves up to 9% of the total global energy and 1.4% of the GNP of gross national products.

Chang et al. (2018) investigated the effects of rubber particle size on the wear and friction of the brake friction materials. They evaluated the frictional performance of this kind of materials which was produced in the size of 75 μm and 450 μm with the recycled rubber particles. They realized that the sample tests with small rubber particles have a higher contact stiffness than the samples which have large rubber particles. However, the small particles increase the friction level and friction instability which leads to a higher wear rate for the sample tests due to larger pressure

contact plateaus at the sliding interface. They concluded that the contact plateaus get significantly affected by the frictional instability of brake friction materials and this can be decreased by adjusting the recycled rubber particle size.

Ismailov et al. (2018) presented an innovative testing system to measure the effects of friction. This machine was the modified version of slurry-type high-speed rubber wheel. They used different values for velocity ranged between 1.7 m/s to 17 m/s to investigate the friction behaviour of the steel material as sample test with irregular roughness against a particular type of rubber under the water lubricated contact. They found a friction maximum for the velocity range of 6.7 to 8.3 m/s where the resulting wear on the sample test was in the highest level of contact. At the higher sliding velocity, the friction was on the lower level with less wear with reduction in frictional heat due to slight improvement in mixed lubrication.

Lin et al. (2018) studied the effects of different fillers which are combined into the pure rubber in order to improve the rubber resistance against wear. This research work is about investigation of rubber properties including mechanical and tribological properties with different composites containing graphene and cellulose nanocrystal. The preformed sliding wear test under dry condition. They found that the combination of graphene and cellulose nanocrystal increases the storage modulus of rubber and reduces the hysteresis loss. They also realized that the normal load and sliding velocity significantly affect the friction and wear properties of the rubber composites.

Chintha et al. (2019) evaluated the role of fracture toughness of a material of steel on impact abrasion. For this purpose, they developed two different alloys of steel having different fracture

toughness and same hardness level. They performed the impact abrasion wear test on the steel alloys and examined the damaged samples. They found that if the fracture toughness of alloy steel is improved, it helps the materials to resist against both impact and abrasion damage.

Zhou et al. (2019) investigated the fretting properties of a rubber seal in hydrogen atmosphere. They presented a numerical model to evaluate the influence of hydrogen swelling and using this model they studied the fretting behaviour of a rubber seal. Their results showed that the fretting state of rubber seal get strongly affected by the amplitude of reciprocating motion and the O ring seal in the hydrogen atmosphere with high pressure has a high tendency to move in the sticking regime due to swelling effect. They claimed that the fatigue failure of rubber seal is progressed in hydrogen atmosphere more than the air atmosphere because of a higher fluctuation range of the peak Mises stress in hydrogen.

Budinski and Budinski (2017) by mentioning the problems which exists in the standard test of ASTM G 65 in some cases, tried to find a replacement test and checked the validity of the ASTM G 174 loop abrasion test. They performed various friction tests on different substrates with rubber wheel which were used for three body abrasion. The aim was to find out the interface between the rubber and abrasive. They also conducted some experiments to replace the rubber wheel for the three body test using a steel wheel. At the end, they tried to correlate the results by the ASTM G 65 tests and the ASTM G 174. They found that the steel wheel cannot be used with the force in ASTM G 65 and the sands crushes and are changed to powder. They also realized that the rubbers have a different interaction with abrasives and substrates.

Alshammari et al. (2018) used a hand lay - up technique to produce epoxy composite according to the jute fiber mates and investigated the material removal from the composite surface when occurring the sliding condition. For this purpose, they considered different applied loads in order to obtain various shear force on the interface and used scanning electron microscopy technique to explore the effects of shear force on the interaction between the fiber and resin after sliding happens along different directions. They found that the fiber direction significantly gets affected by the wear and frictional performance of jute fiber reinforced epoxy composites. When the composite is tested in parallel and antiparallel directions, this is the sliding distance which controls the wear behavior of the composite.

Singh Gill and Yousif (2009) in an experimental research work, used betel nut fibers as reinforcement for tribo-polyester composite. They fabricated the composites with 13 layers of betel nut fiber mats which were distributed in a random way and 15 layers of polyester. They investigated the wear and frictional behaviors of the composite against a counterface of polished stainless steel using a new block-on-disc BOD machine. It was concluded that using betel nut fiber in the composite increases the wear performance up until 98 % and frictional performance by about 73 %.

Yousif (2012) proposed glass fiber as synthetic and palm oil fiber as natural reinforcements for polyester composites and adopted a new technique for fabrication of chopped strand, mat glass fiber-reinforced polyester composite (FRPC). He used a compressed mold to produce palm oil fiber-reinforced polyester (PORP) composites and developed two PORP composites based on untreated or treated (with 6% NaOH) palm oil fibers. Moreover, he produced a neat polyester material to study the influence of each fiber on its tribo-performance.

Hakami et al. (2019) investigated the abrasion wear of different rubber materials such as styrene butadiene rubber (SBR), natural rubber (NR) and nitrile butadiene rubber (NBR). These rubber types were tested while sliding over abrasives with different sizes and the tests were performed at different normal loads. They selected different properties such as tensile strength and elongation at break as the input parameters. They found that the tribological system is not the only factor affecting the wear of rubber. The mechanical properties of rubber which contribute different wear mechanisms are also important.

Chapter 3. Methodology

3.1 Introduction

This chapter presents the details and method which are used to perform experiments for abrasion wear in rubber samples. In fact, it consists of a series of tests in three body abrasion of rubber under dry contact condition. The explanations about the testing machine which is available in USQ are also given.

The testing machine which is used for the experimental work in this thesis was designed and fabricated by Yousif (2013). He presented a fabricated tribological testing machine for performing wear and frictional experiments under dry and wet condition. He introduced a new concept of collecting more than one tribo-technique for various types of contact (area, line or point contact) which was able to work at the same time under the same test condition and same material. The important feature of the presented testing machine is that it is able to perform tests with different wear modes including adhesive, two and three-body-abrasive under different conditions of dry, lubricated or slurry.

Figure 3.1 presents a schematic of this testing machine which is used to perform experimental tests in this thesis. As indicated in this figure, the main components of this machine are: 1. counterface, 2. block on ring (BOR) load lever, 3. block on disk (BOD) load lever, 4. third body hopper, 5. BOD specimen, 6. BOR specimen, 7. lubricant container and 8. dead weights.

In this testing machine, several load cells are installed on the BOR and BOD load levers to measure the magnitude of the frictional forces which are generated between the specimens and the

counterface. The load cells with the type of Accutec B6 N-50 and Accutec H3-50 are integrated with a weight indicator in order to read the friction forces at the same time.

In order to measure the interface temperature, some infrared thermometers are connected to the frame of the testing machine and directed to the rubbing surface area. This machine is able to perform BOR load lever and BOD load lever technique or a combination of these two against the same counterface at the same time.

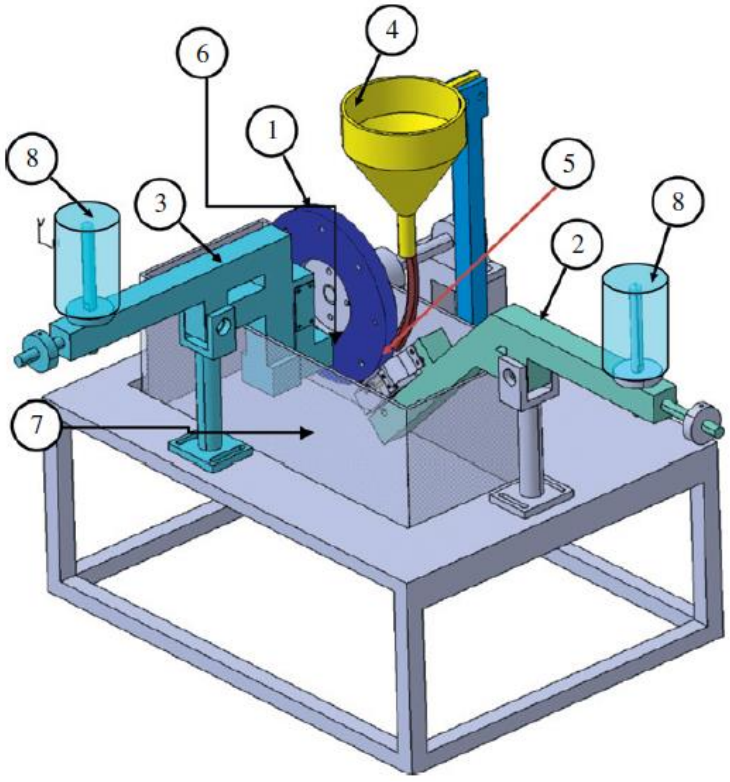

Figure 3.1. Schematic of testing machine used for experimental tests in this thesis (Yousif, 2013)

Apart from performing the adhesive tests, this machine can also provide tests for three-abrasion under dry condition using the abrasives of sand and steel wheel configuration or sand and rubber wheel configuration. Table 3.1 presents some of technical specifications of this machine.

Table 3.1. Specifications of the testing machine (Yousif, 2013)

Part	Specification
Wheel speed	5–2000 rpm
Wheel type	6.65” Steel wheel as per ASTM B 611 9” Rubber wheel as per ASTM G 65
Load	5-500 N
Motor type	AC motor with frequency inverter drive
Specimen size	25 mm × 58 mm for BOR 10 mm × 10 mm for BOD
Specimen thickness	6 – 20 mm
Test types	ASTM (G65, G105, B611, G137-95 and G77)

Figure 3.2 shows a photo of this testing machine for adhesive test under dry contact condition. This machine allows researchers to conduct adhesive tests with block on disk BOD and block on ring BOR at the same time against a counterface surface. The block on ring technique is performed based on the ASTM G77-98 and the block on disc method based on ASTM G99.

For the dry contact condition, adhesive wear test is conducted against a ring made of stainless steel (AISI 304). Before performing any test, the disc should be first polished with abrasive Silicon Carbide (SiC) paper to a surface roughness of 0.1–0.3 μm Ra. Meanwhile, the specimen is also rubbed over the SiC paper. It is to make sure that there is a close contact between the sliding face of the specimen and the stainless steel ring. The sliding test is carried out at local

temperature and humidity conditions with normal loads range from 10 N to 500 N, sliding speeds from 2.8 m/s to 3.9 m/s, and sliding distances of 0 to 7 km (Yousif, 2013).

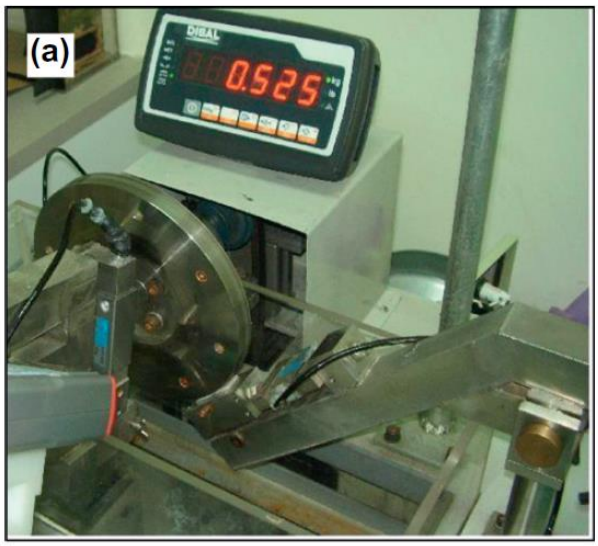

Figure 3.2. photograph of the testing machine for adhesive test under dry condition (Yousif, 2013)

3.2 Experimental procedure

The experiments in this research work were performed at dry contact condition. The nitrile rubber specimens were prepared and inserted into device. Instead of stainless steel ring, the tests were conducted with aluminium ring. The weight of rubber specimens was measured before and after of any test. The tests were performed with speed of 2.2 m/s, 2.6 m/s and 3 m/s. The normal loads were varied from 10 N to 40 N with 10 N intervals. It means the normal loads of 10 N, 20 N, 30 N and 40 N.

The duration of each experiment was 10 minutes. The amount of frictional force was recorded in 1 minute intervals. After every 2 minutes, the test was stopped to record the weight of the specimen to compare it with initial weight. Three set of tests were performed on the whole in

this research work for the speeds of 2.2, 2.6 and 3 m/s. For each speed, four different tests for the normal loads of 10, 20, 30 and 40 N were conducted. The results of these experiments will be presented in the next chapter.

Figures 3.3 and 3.4 shows the specimen in the testing machine and rubber sample before and after adhesive wear. As it is seen in Fig. 3.3, some of the rubber particles are removed from the specimen due to sliding the aluminium ring on the rubber. The amount of this lost material can be obtained by measuring the weight of rubber specimen before and after the test.

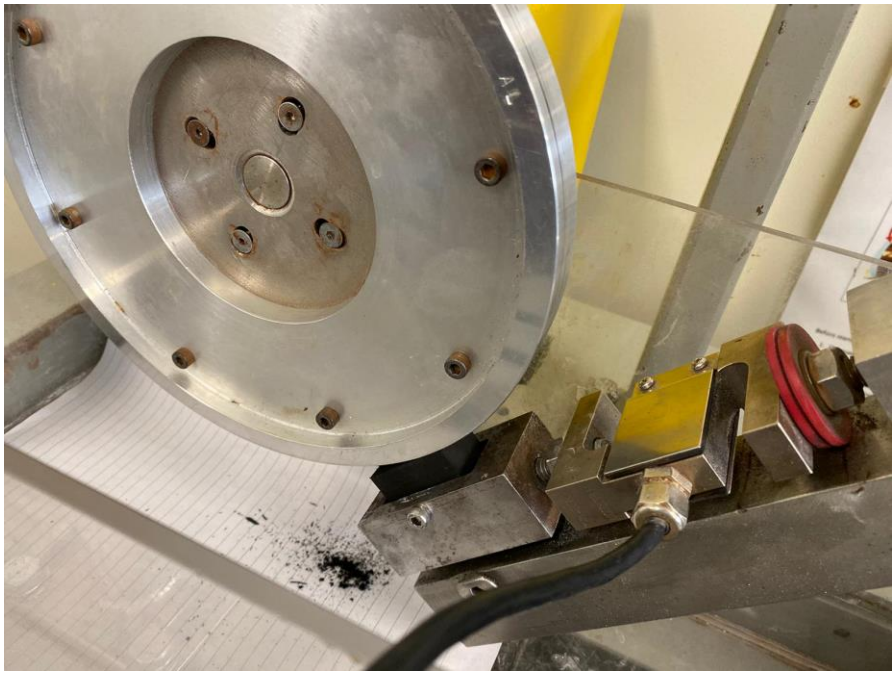

Figure 3.3. Rubber specimen in the testing machine

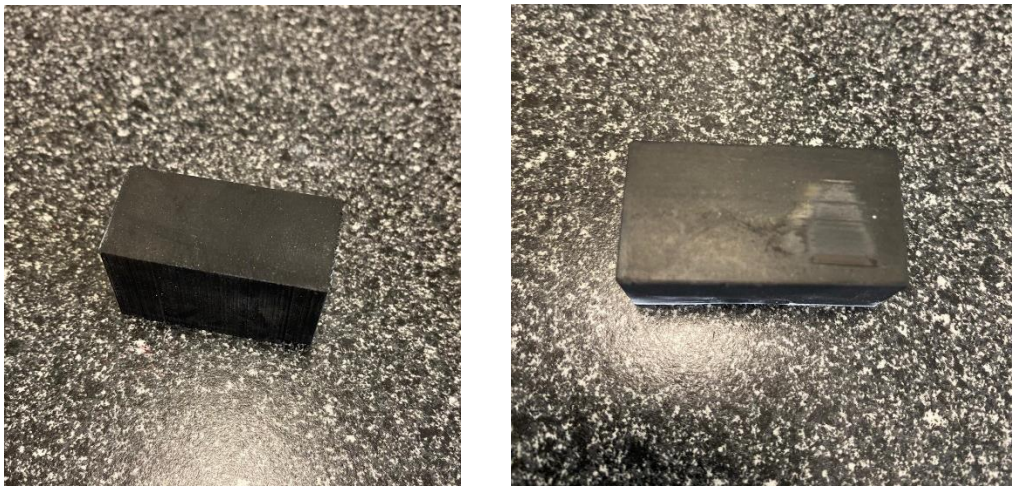

(a) *(b)*

Figure 3.4. Rubber specimen; (a) before experiment, (b) after experiment

3.3. Scanning electron microscope (SEM) observations

As another task of this research work, SEM was used to observe the surface morphology on the rubber and bonding area after conducting the experiments. This technique can help with a better understanding of wear process in rubber material by providing a very high resolution images of the worn rubber. The microstructure of the rubber samples, as well as worn surfaces of can be studied using SEM.

The samples for the SEM were prepared on a small EM holder and fixed using a liquid carbon and double-sided carbon tape. The sample was then placed in a smart coater machine about 1 minute for each sample. After that the sample was placed in the SEM chapter for evacuation process. It took a while to get the image into the computer. The computer has software which is integrated to the SEM enabling to capture the images and save it on the computer.

Chapter 4. Results and discussions

4.1 Introduction

This chapter presents the results and analysis of experimental data which were obtained by performing adhesive wear tests on rubber sample. The sample material was nitrile with a density of 250 kg/m^3. Three sets of experiments were conducted for three different speeds of 2.2, 2.6 and 3 m/s of the linear velocity of the aluminium wheel. For each speed, the sample was tested for four normal loads of 10, 20, 30 and 40 N.

Each test lasted for 10 minutes. Different data were recorded at every 2 minute intervals including the weight of the samples before and after the test, frictional force at every minute. It should be mentioned that the specimen was replaced with a new one for performing test for each normal load. The obtained data together with calculations of volume loss and specific wear rate are presented in the flowing sections.

4.2 Measured data

The recorded data are given in this section. Tables 4.1 to 4.6 present measured data for the speeds of 2.2, 2.6 and 3 m/s. Calculations of distance, volume loss and the specific wear rate in these tables are performed based on the following equations:

$$\text{Sliding distance} = \text{speed} \times \text{time} \times 60 / 1000$$

$$\text{Volume loss} = \text{weight loss} / \text{density}$$

$$\text{Specific wear rate (SWR)} = \text{volume loss} / (\text{sliding distance} \times \text{normal load} \times 1000)$$

Table 2.1. Measured data for speed 2.2 m/s

sample	Normal load (N)	Time (min.)	Distance (km)	Weight before	Weight after	Weight loss (g)	Volume loss (mm^3)	Specific wear rate
Sample 1	10	2	0.264	20.8275	20.8273	0.0002	8E-07	3.03E-10
		4	0.528	20.8275	20.824	0.0035	1.4E-05	2.652E-09
		6	0.792	20.8275	20.819	0.0085	3.4E-05	4.293E-09
		8	1.056	20.8275	20.8169	0.0106	4.24E-05	4.015E-09
		10	1.32	20.8275	20.8104	0.0171	6.84E-05	5.182E-09
Sample 2	20	2	0.264	20.8032	20.7883	0.0149	5.96E-05	1.129E-08
		4	0.528	20.8032	20.7602	0.043	0.000172	1.629E-08
		6	0.792	20.8032	20.734	0.0692	0.0002768	1.747E-08
		8	1.056	20.8032	20.7263	0.0769	0.0003076	1.456E-08
		10	1.32	20.8032	20.7183	0.0849	0.0003396	1.286E-08
Sample 3	30	2	0.264	22.2033	22.1643	0.039	0.000156	1.97E-08
		4	0.528	22.2033	22.0875	0.1158	0.0004632	2.924E-08
		6	0.792	22.2033	22.0087	0.1946	0.0007784	3.276E-08
		8	1.056	22.2033	21.8918	0.3115	0.001246	3.933E-08
		10	1.32	22.2033	21.8001	0.4032	0.0016128	4.073E-08
Sample 4	40	2	0.264	21.7998	21.7845	0.0153	6.12E-05	5.795E-09
		4	0.528	21.7998	21.7547	0.0451	0.0001804	8.542E-09
		6	0.792	21.7998	21.71	0.0898	0.0003592	1.134E-08
		8	1.056	21.7998	21.6874	0.1124	0.0004496	1.064E-08
		10	1.32	21.7998	21.6321	0.1677	0.0006708	1.27E-08

Table 4.2. Frictional force for speed 2.2 m/s

sample	Normal load (N)	Time (min.)	0 min.	2^{nd} min.	3^{rd} min.	4^{th} min.	5^{th} min.	6^{th} min.	7^{th} min.	8^{th} min.	9^{th} min.	10^{th} min.	Fric. coef.
Sample 1	10	2	7.539	8.078									0.539
		4	7.528	8.29	8.307	8.334							0.782
		6	7.698	8.325	8.335	8.317	8.364	8.339					0.638
		8	7.562	8.414	8.415	8.824	8.416	8.824	8.438	8.402			0.971
		10	7.543	8.406	8.377	8.409	8.418	8.395	8.428	8.371	8.379	8.381	0.853
Sample 2	20	2	7.622	8.848									0.613
		4	7.615	8.847	8.849	8.852							0.617
		6	7.647	8.862	8.873	8.875	8.905	8.902					0.618
		8	7.601	9.278	9.157	9.218	9.211	9.199	9.204	9.227			0.806
		10	7.632	9.281	9.267	9.242	9.24	9.242	9.233	9.223	9.258	9.267	0.809
Sample 3	30	2	7.722	9.461									0.579
		4	7.743	9.499	9.524	9.533							0.592
		6	7.712	9.687	9.652	9.647	9.68	9.658					0.651
		8	7.732	9.649	9.68	9.662	9.679	9.672	9.638	9.652			0.643
		10	7.736	9.721	9.685	9.69	9.675	9.703	9.701	9.71	9.709	9.712	0.655
Sample 4	40	2	7.786	10.004									0.554
		4	7.808	9.968	9.998	9.977							0.543
		6	7.771	9.916	9.91	9.877	9.897	9.912					0.533
		8	7.814	9.889	9.871	9.896	9.883	9.869	9.874	9.86			0.516
		10	7.809	9.997	10.02	10.00	10.01	10.03	10.02	10.01	10.02	10.02	0.552

Table 4.3. Measured data for speed 2.6 m/s

sample	Normal load (N)	Time (min.)	Distance (km)	Weight before	Weight after	Weight loss (g)	Volume loss (mm^3)	Specific wear rate
Sample 1	10	2	0.312	24.7296	24.7211	0.0085	3.4E-05	1.09E-08
		4	0.624	24.7296	24.7245	0.0051	2.04E-05	3.269E-09
		6	0.936	24.7296	24.7047	0.0249	9.96E-05	1.064E-08
		8	1.248	24.7296	24.6924	0.0372	0.000149	1.192E-08
		10	1.56	24.7296	24.6812	0.0484	0.000194	1.241E-08
Sample 2	20	2	0.312	26.0576	26.0568	0.0008	3.2E-06	5.128E-10
		4	0.624	26.0576	26.0463	0.0113	4.52E-05	3.622E-09
		6	0.936	26.0576	26.0376	0.02	8E-05	4.274E-09
		8	1.248	26.0576	26.004	0.0536	0.000214	8.59E-09
		10	1.56	26.0576	25.9459	0.1117	0.000447	1.432E-08
Sample 3	30	2	0.312	25.9459	25.9427	0.0032	1.28E-05	1.368E-09
		4	0.624	25.9459	25.9372	0.0087	3.48E-05	1.859E-09
		6	0.936	25.9459	25.9065	0.0394	0.000158	5.613E-09
		8	1.248	25.9459	25.8433	0.1026	0.00041	1.096E-08
		10	1.56	25.9459	25.7794	0.1665	0.000666	1.423E-08
Sample 4	40	2	0.312	25.7079	25.6819	0.026	0.000104	8.333E-09
		4	0.624	25.7079	25.6293	0.0786	0.000314	1.259E-08
		6	0.936	25.7079	25.5727	0.1352	0.000541	1.444E-08
		8	1.248	25.7079	25.4555	0.2524	0.00101	2.022E-08
		10	1.56	25.7079	25.3859	0.322	0.001288	2.064E-08

Table 4.4. Frictional force for speed 2.6 m/s

sample	Normal load (N)	Time (min.)	0 min.	2^{nd} min.	3^{rd} min.	4^{th} min.	5^{th} min.	6^{th} min.	7^{th} min.	8^{th} min.	9^{th} min.	10^{th} min.	Fric. coef.
Sample 1	10	2	7.452	8.274									0.822
		4	7.431	8.298	8.306	8.308							0.873
		6	7.456	8.235	8.234	8.227	8.236	8.242					0.779
		8	7.463	8.308	8.326	8.337	8.282	8.302	8.318	8.267			0.843
		10	7.466	8.383	8.337	8.333	8.31	8.322	8.332	8.315	8.31	8.297	0.861
Sample 2	20	2	7.589	8.942									0.677
		4	7.579	9.068	9.029	9.023							0.731
		6	7.609	9.008	8.997	9.014	9.001	8.987					0.696
		8	7.601	8.942	8.924	8.918	8.93	8.91	8.938	8.927			0.663
		10	7.599	8.957	8.952	8.954	8.966	8.968	8.985	8.968	8.979	8.997	0.685
Sample 3	30	2	7.72	10.002									0.761
		4	7.718	10.081	10.04	10.08							0.784
		6	7.73	9.681	9.695	9.734	9.775	9.765					0.667
		8	7.709	9.731	9.736	9.739	9.746	9.781	9.77	9.748			0.68
		10	7.747	9.838	9.748	9.763	9.755	7.775	9.789	9.776	9.783	9.774	0.603
Sample 4	40	2	7.802	10.285									0.621
		4	7.813	10.268	10.23	10.32							0.621
		6	7.831	10.389	10.36	10.37	10.36	10.35					0.634
		8	7.812	10.173	10.13	10.19	10.22	10.21	10.22	10.22			0.596
		10	7.822	10.337	10.34	10.34	10.35	10.32	10.38	10.31	10.29	10.37	0.629

Table 4.5. Measured data for speed 3 m/s

sample	Normal load (N)	Time (min.)	Distance (km)	Weight before	Weight after	Weight loss (g)	Volume loss (mm^3)	Specific wear rate
Sample 1	10	2	0.36	25.3859	25.3853	0.0006	2.4E-06	6.667E-10
		4	0.72	25.3859	25.3739	0.012	4.8E-05	6.667E-09
		6	1.08	25.3859	25.3317	0.0542	0.0002168	2.007E-08
		8	1.44	25.3859	25.2773	0.1086	0.0004344	3.017E-08
		10	1.8	25.3859	25.2253	0.1606	0.0006424	3.569E-08
Sample 2	20	2	0.36	22.3487	22.3386	0.0101	4.04E-05	5.611E-09
		4	0.72	22.3487	22.3169	0.0318	0.0001272	8.833E-09
		6	1.08	22.3487	22.2745	0.0742	0.0002968	1.374E-08
		8	1.44	22.3487	22.2309	0.1178	0.0004712	1.636E-08
		10	1.8	22.3487	22.1817	0.167	0.000668	1.856E-08
Sample 3	30	2	0.36	22.1817	22.1563	0.0254	0.0001016	9.407E-09
		4	0.72	22.1817	22.0998	0.0819	0.0003276	1.517E-08
		6	1.08	22.1817	22.0524	0.1293	0.0005172	1.596E-08
		8	1.44	22.1817	22.0107	0.171	0.000684	1.583E-08
		10	1.8	22.1817	21.9639	0.2178	0.0008712	1.613E-08
Sample 4	40	2	0.36	24.8687	24.8515	0.0172	6.88E-05	4.778E-09
		4	0.72	24.8687	24.8246	0.0441	0.0001764	6.125E-09
		6	1.08	24.8687	24.8084	0.0603	0.0002412	5.583E-09
		8	1.44	24.8687	24.7883	0.0804	0.0003216	5.583E-09
		10	1.8	24.8687	24.7778	0.0909	0.0003636	5.05E-09

Table 4.6. Frictional force for speed 3 m/s

sample	Normal load (N)	Time (min.)	0 min.	2nd min.	3rd min.	4th min.	5th min.	6th min.	7th min.	8th min.	9th min.	10th min.	Fric. coef.
Sample 1	10	2	7.677	8.346									0.669
		4	7.659	8.364	8.352	8.362							0.7
		6	7.643	8.32	8.324	8.325	8.32	8.327					0.68
		8	7.655	8.305	8.303	8.315	8.314	8.31	8.322	8.335			0.66
		10	7.668	8.32	8.322	8.316	8.308	8.327	8.322	8.321	8.324	8.323	0.652
Sample 2	20	2	7.732	8.999									0.634
		4	7.766	8.954	8.969	8.944							0.595
		6	7.745	8.879	8.888	8.897	8.875	8.906					0.572
		8	7.734	8.923	8.91	8.93	8.916	8.956	8.93	8.912			0.596
		10	7.752	8.998	9.022	8.983	8.971	8.96	8.945	8.973	8.959	8.953	0.611
Sample 3	30	2	7.886	9.591									0.568
		4	7.845	9.521	9.542	9.517							0.561
		6	7.832	9.536	9.506	9.596	9.54	9.517					0.569
		8	7.874	9.604	9.56	9.583	9.596	9.599	9.567	9.625			0.572
		10	7.833	9.594	9.617	9.675	9.555	9.556	9.499	9.539	9.51	9.489	0.575
Sample 4	40	2	7.889	10.075									0.547
		4	7.909	10.088	10.09	10.06							0.543
		6	7.878	10.121	10.11	10.11	10.11	10.12					0.559
		8	7.895	10.363	10.32	10.37	10.21	10.34	10.24	10.34			0.604
		10	7.904	10.375	10.42	10.21	10.36	10.39	10.37	10.35	10.33	10.32	0.611

4.3 Adhesive wear plots

This section presents the plots for adhesive wear tests on the rubber samples. Different plots including distance against volume loss, distance against specific wear rate and distance against friction coefficient are presented. These set of plots are given for the test speeds of 2.2, 2.6 and 3 m/s based on different normal loads of 10, 20, 30 and 40 N. At the end, results comparison for different parameters based on different speeds are presented.

4.3.1 Speed of 2.2 m/s

Figure 4.1 shows the volume loss plot against the distance for speed 2.2 m/s. It includes curves for different loads. As it is seen, the amount of volume loss increases with sliding distance. This trend exists for all applied normal loads. The maximum volume loss is around 0.0016 mm^3 for the 30 N normal load.

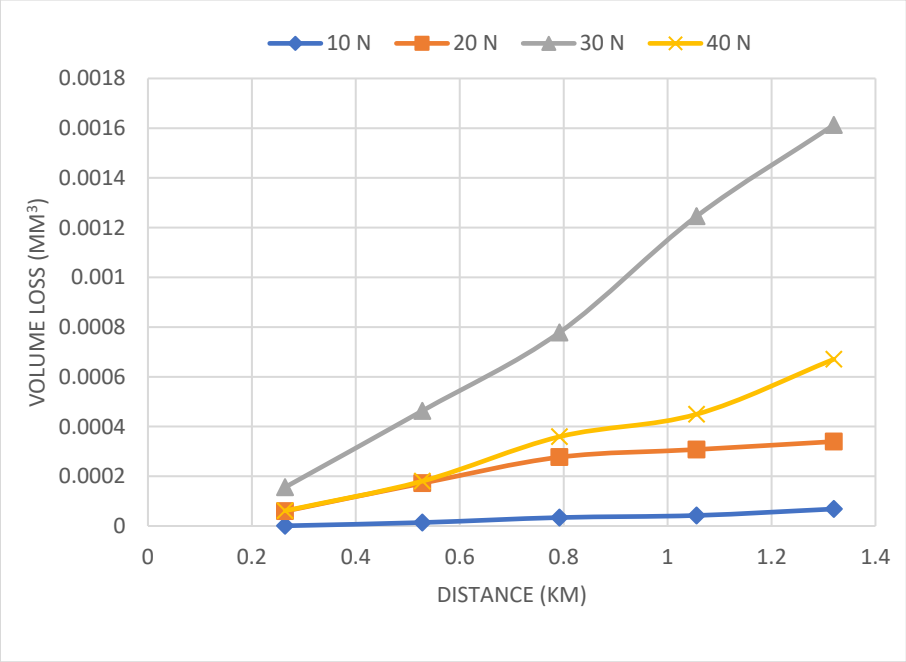

Figure 4.1. Distance vs. volume loss for speed 2.2 m/s

The plot of specific wear rate for the speed of 2.2 m/s is given in Fig. 4.2. The trend is proportional with the volume loss. The 30 N load which causes the maximum value of volume loss, makes the highest SWR. The highest wear rate is around 4×10^{-8} $mm^3/N.m$ for this load. The curves have almost an increasing trend with sliding distance.

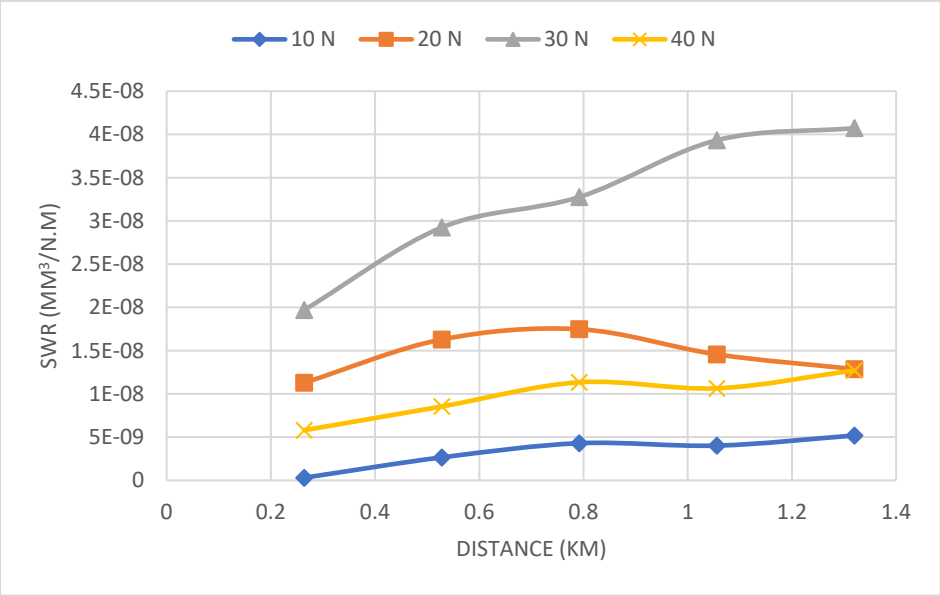

Figure 4.2. Distance vs. specific wear rate for speed 2.2 m/s

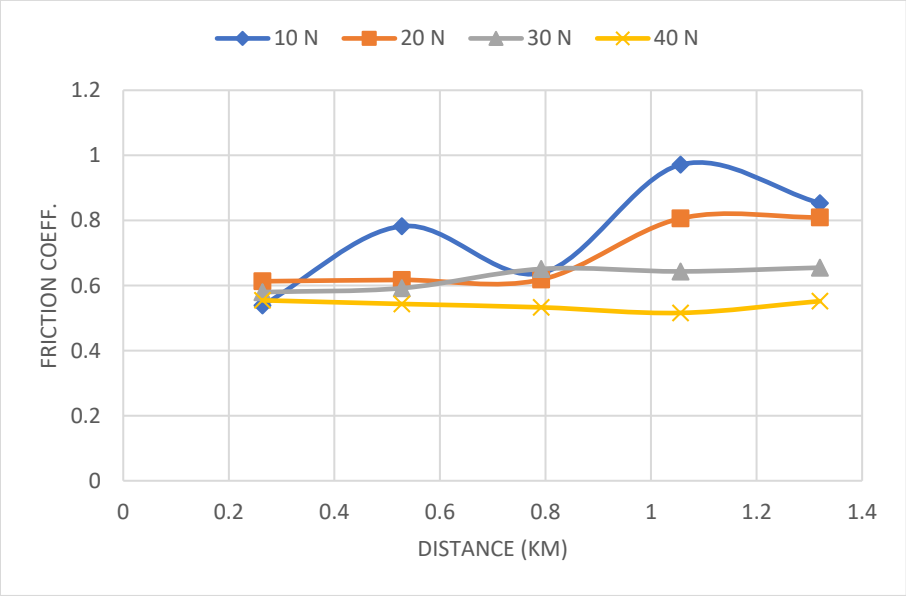

Figure 4.3. Distance vs. average friction coefficient for speed 2.2 m/s

Plots for friction coefficient against sliding distance for speed of 2.2 m/s is shown in Fig. 4.3. The friction coefficient has a reverse relation with the applied normal load. As the normal load increase, the friction coefficient decreases. As it is observed in Fig. 4.3, the highest value of the friction coefficient with the amount of around 1 belongs to the normal load of 10 N. And the lowest value of around 0.5 for the normal load of 40 N.

4.3.2 Speed of 2.6 m/s

Figure 4.4 shows the plot of volume loss against the sliding distance for speed of 2.6 m/s for normal loads of 10, 20, 30 and 40 N. It is observed that the highest amount of volume loss happens for the highest normal load of 40 N with the amount of 0.0013 mm^3. This is due to the fact that the increase in the mechanical loadings in the interface, leads to a higher material removal from the soft body. All curves have an increasing trend with sliding distance.

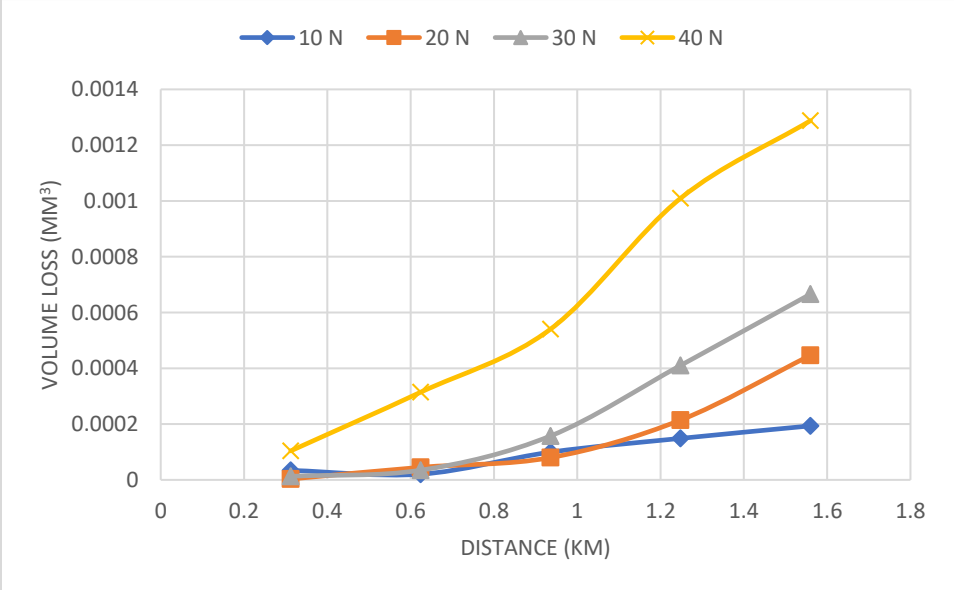

Figure 4.4. Distance vs. volume loss for speed 2.6 m/s

The specific wear rate against sliding distance for speed of 2.6 m/s is plotted in Fig. 4.5. It can be seen that all curves for the normal loads have almost an increasing trend with sliding distance. The 40 N normal load which caused the maximum value of volume loss. The highest magnitude of SWR is around 2.1×10^{-8} $mm^3/N.m$ at the end of sliding distance for this normal load.

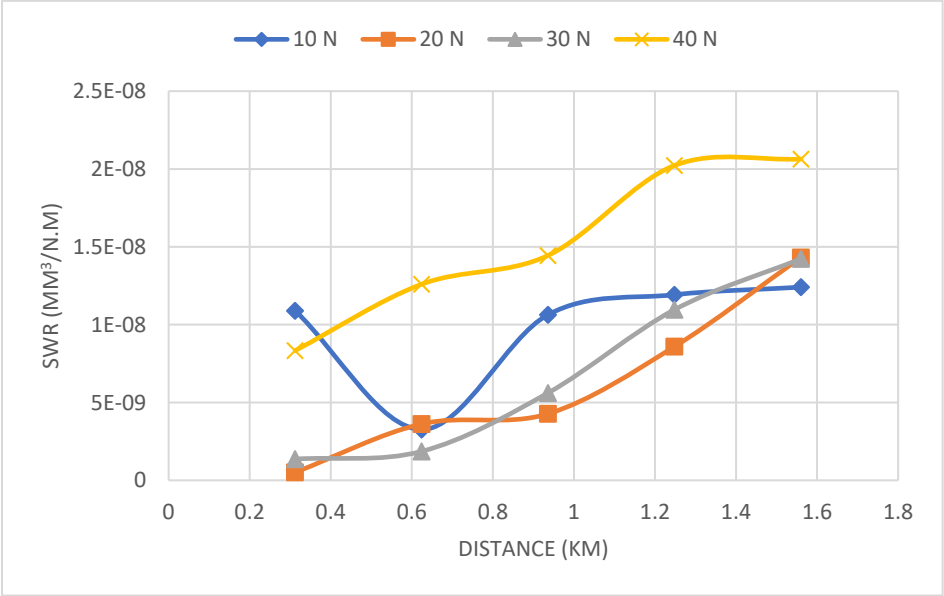

Figure 4.5. Distance vs. specific wear rate for speed 2.6 m/s

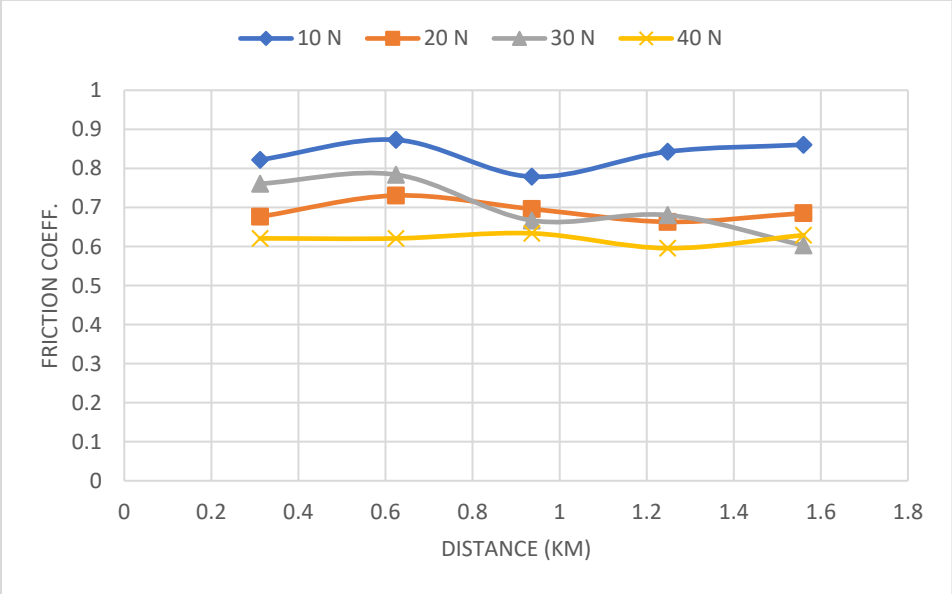

Figure 4.6. Distance vs. average friction coefficient for speed 2.6 m/s

Figure 4.6 shows the plot of friction coefficient against sliding distance for the test speed of 2.6 m/s. It is observed that the friction coefficient remains almost constant with minimum deviation at each load. The amount of friction coefficient reduces with increasing the applied normal load. For the normal load of 10 N, the average friction coefficient is around 0.85, while it is around 0.63 for the 40 N load.

4.3.3 Speed of 3 m/s

Plot of volume loss against sliding distance for the speed of 3 m/s is shown in Fig. 4.7 for different normal loads. It can be seen that all curves have an increasing trend with sliding distance. The highest volume loss is for the 30 N load with a value of around 0.00088 mm^3. All curves start with a value of less than 0.0001 mm^3 and then increase by increasing the sliding distance.

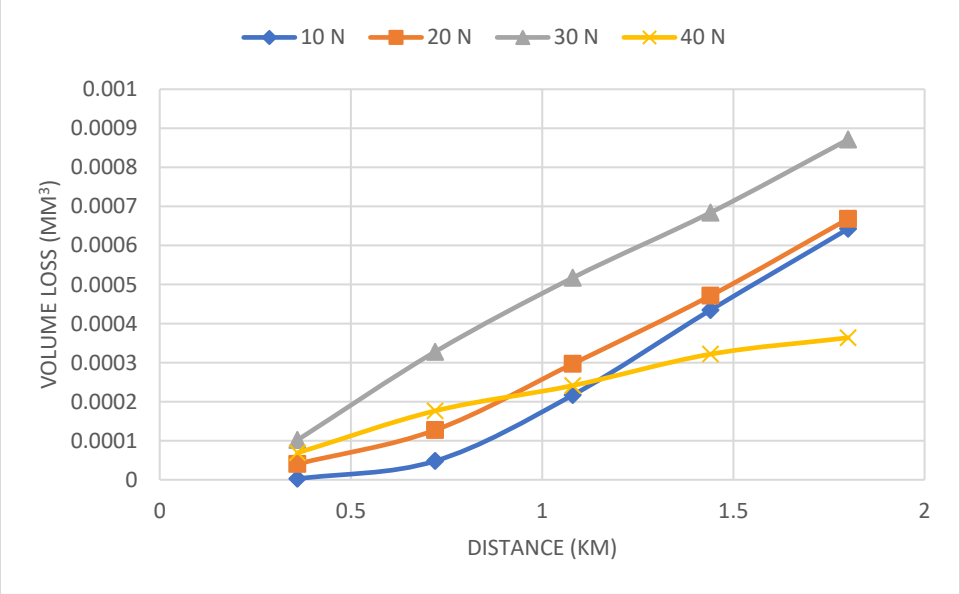

Figure 4.7. Distance vs. volume loss for speed 3 m/s

For the case of specific wear against sliding distance, the plot for the speed of 3 m/s is given in Fig. 4.8 for different normal loads. The curves have almost an increasing trend with sliding distance. The maximum value for the specific wear rate happens at the normal load of 10 N with an amount of around 3.5×10^{-8} $mm^3/N.m$.

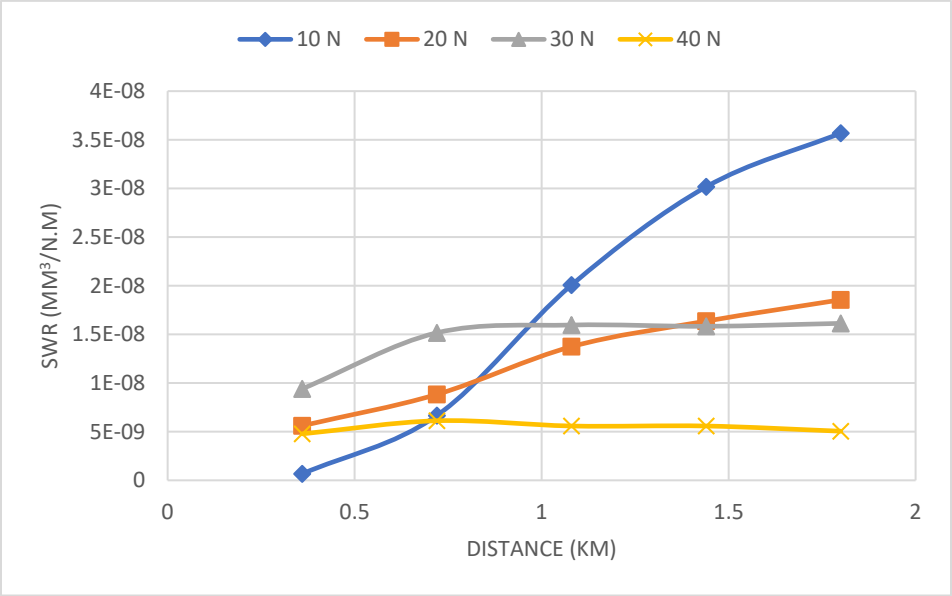

Figure 4.8. Distance vs. specific wear rate for speed 3 m/s

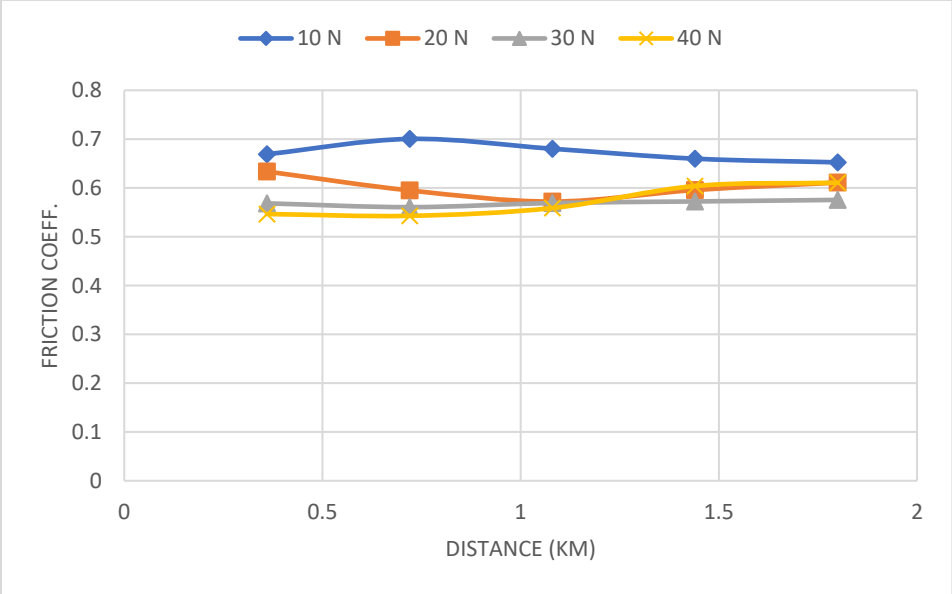

Figure 4.9. Distance vs. average friction coefficient for speed 3 m/s

Figure 4.9 indicates the value of friction coefficient against the sliding distance at the speed of 3 m/s for the various loads. Similar the trends for previous speeds, an almost constant friction coefficient exists for the curves of different normal loads. And the maximum magnitude of the friction coefficient belongs to the minimum normal load of 10 N with the amount of around 0.77. The lowest magnitude for the friction coefficient happens for the highest normal load of 40 N with a value of around 0.55.

4.3.4 Results comparison

The comparison of the results is presented in this section. The effects of normal load of the measured parameters including volume loss, specific wear rate and friction coefficient were investigated in the previous sections. Here the effect of test speed on these parameters is investigated while the normal load remains constant. The comparison is made for the sample 2 with the normal load of 20 N.

Figure 4.10 shows the plot of volume loss against sliding distance at the normal load of 20 N for different test speeds. It can be seen that the volume loss increases with increasing of sliding distance. It is also observed that the test speed affects the value of volume loss. The maximum volume loss happens for the highest test speed of 3 m/s with a magnitude of around 0.00067 mm^3. The volume loss is initially maximum for the test speed of 2.2 m/s but its trend changes gradually and reaches its maximum value for the speed of 3 m/s at the end of sliding distance.

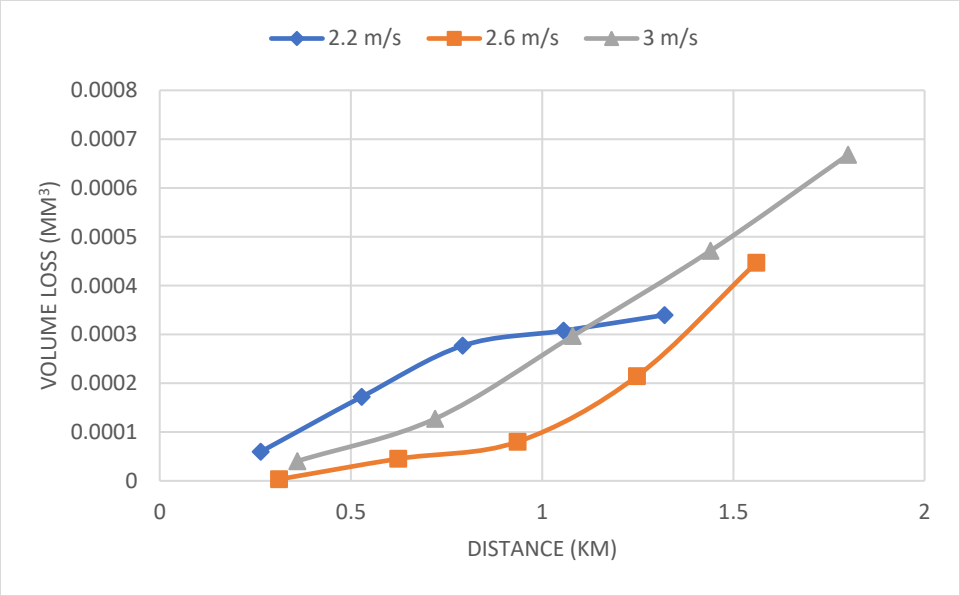

Figure 4.10. Distance vs. volume loss for different speeds at normal load of 20 N

The specific wear rate is plotted against the sliding distance for three test speeds in Fig. 4.11. The normal load is fixed at 20 N. similar to the trend for the volume loss, the SWR is maximum for the speed of 2.2 m/s at the start of sliding distance. This trend changes and the maximum SWR with a value of around 1.8×10^{-8} happens for the speed of 3 m/s at the end of sliding distance.

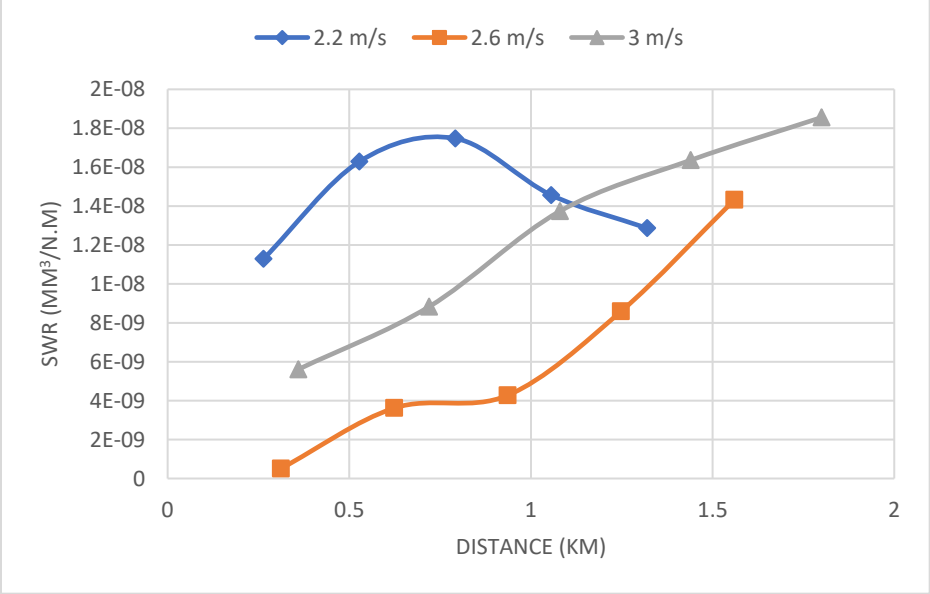

Figure 4.11. Distance vs. specific wear rate for different speeds at normal load of 20 N

Figure 4.12 shows the plot of friction coefficient against sliding distance for three test speeds at the constant normal load of 20 N. It is observed that there is no significant change in the value of friction coefficient at each speed. The maximum value of friction coefficient happened at the speed of 2.2 m/s with a value of around 0.81.

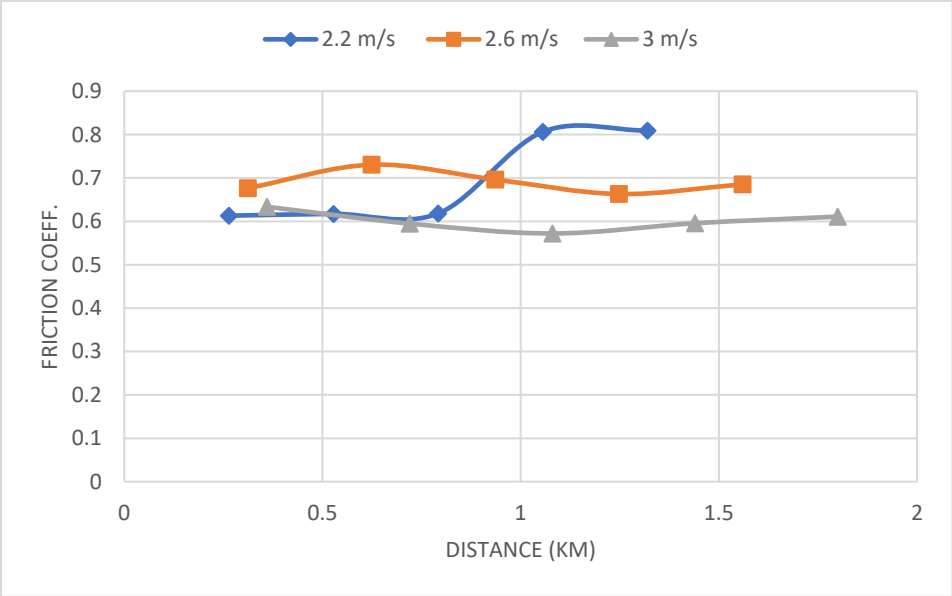

Figure 4.12. Distance vs. average friction coefficient for different speeds at normal load of 20 N

4.4 SEM observations

Figure 4.13 shows different images of worn rubber samples using SEM techniques integrated with the testing machine. These images were taken for the rubber samples under test speed of 2.2 m/s and normal loads of 10 N and 40 N. Wear effects on the rubber samples are obvious in these images. The intensity of wear becomes more as the test speed of applied normal loads increase.

(a)

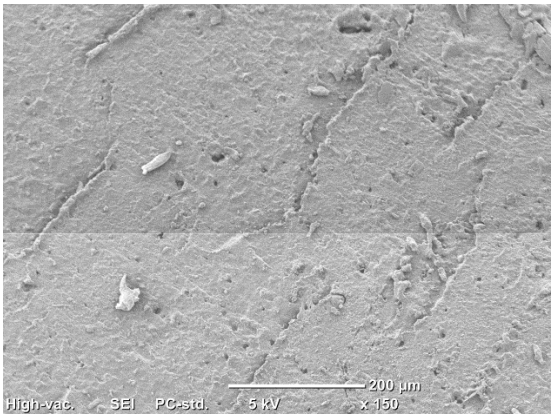

(b)

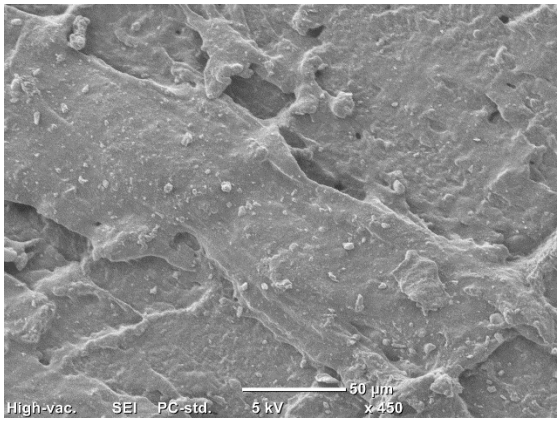

(c)

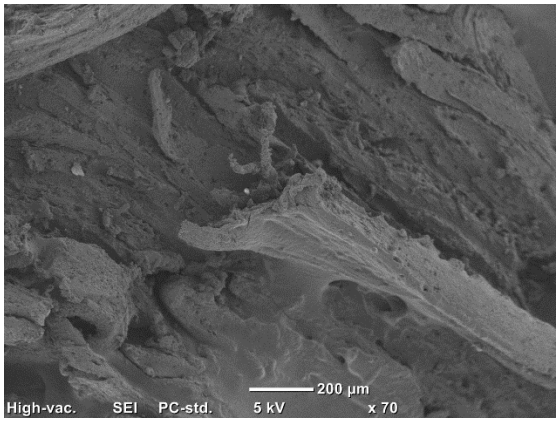

(d)

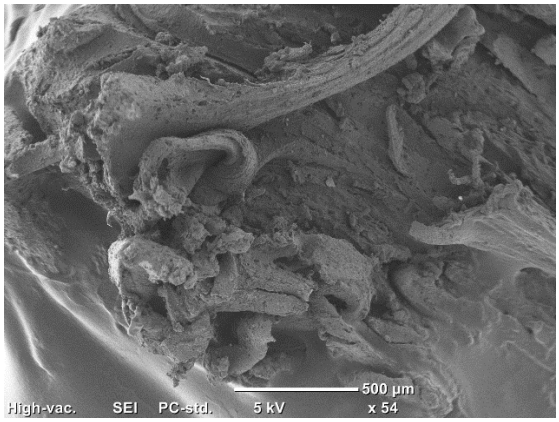

(e)

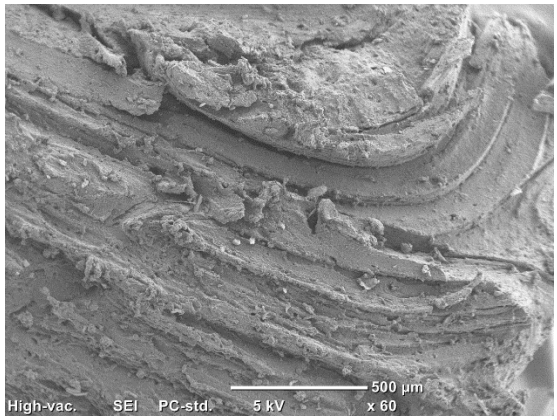

(f)

Figure 4.13. SEM micrographs of the rubber sample

Chapter 5. Conclusions

The adhesive wear test was performed on rubber sample in this research work. The experiments were carried out under different speeds of 2.2, 2.6 and 3 m/s and different normal loads of 10, 20, 30 and 40 N. Wear parameters including volume loss, specific wear rate and average friction coefficient were investigated. Test results were plotted against sliding wear for each parameter in the previous section.

Based on the obtained results, it was seen that the volume loss is almost proportional to the magnitude of the normal force. The higher normal force causes a larger amount of volume loss on the rubber sample. The amount of volume loss is also proportional to the sliding distance. As the sliding distance increases, a higher amount of rubber is removed from the sample.

It was observed that the specific wear rate has almost a similar trend to the volume loss. This is proportional to the magnitude of sliding distance. The specific wear rate increases by increasing the sliding distance. Its magnitude is also dependent to the applied normal load. The normal loads of 30 and 40 N, lead to the higher value of SWR.

For the case of average friction factor, it was observed that the value of this coefficient remains almost constant with sliding distance. It means the magnitude of the friction coefficient does not experience a significant change during the sliding process. It was seen that the normal load makes a reverse effect on the magnitude of the friction coefficient. The lower normal load causes a higher friction coefficient for the sample.

Further comparisons were made for the results based on the test speed by keeping the normal load constant. For the volume loss and specific wear rate parameters, it was seen that their

magnitudes are higher for the lowest test speed at the beginning stages of sliding distance. But this trend changes and their magnitudes get higher for the highest test speed at the end of sliding process.

For the case of friction coefficient with the test speeds, it was observed that the higher test speeds make a larger friction coefficient at the early stages of sliding process. However, this trend changes by reaching to the late stages and the lowest test speed causes the highest magnitude of the friction coefficient.

On the whole, it is concluded that the adhesive wear parameters such as volume loss, specific wear rate and average friction coefficient depend significantly on the factors such as test speed, the applied normal load and sliding distance.

References

AFFATATO, S. & BRANDO, D. 2013. Introduction to wear phenomena of orthopaedic implants. *Wear of Orthopaedic Implants and Artificial Joints.* Elsevier.

AGHABABAEI, R., WARNER, D. H. & MOLINARI, J.-F. 2016. Critical length scale controls adhesive wear mechanisms. *Nature communications,* 7**,** 11816.

AGHABABAEI, R., WARNER, D. H. & MOLINARI, J.-F. 2017. On the debris-level origins of adhesive wear. *Proceedings of the National Academy of Sciences,* 114**,** 7935-7940.

ALSHAMMARI, F., SALEH, K., YOUSIF, B., ALAJMI, A., SHALWAN, A. & ALOTAIBI, J. 2018. The Influence of Fibre Orientation on Tribological Performance of Jute Fibre Reinforced Epoxy Composites Considering Different Mat Orientations. *Tribology in Industry,* 40.

APPLERUBBER. 2019. *Measuring adhesiveness with ASTM D429 Method C* [Online]. Available: https://www.applerubber.com/hot-topics-for-engineers/measuring-adhesiveness-with-astm-d429-method-c-photos/.

ARCHARD, J. 1980. Wear theory and mechanisms. *Wear control handbook,* 58.

BRINK, T. & MOLINARI, J.-F. 2019. Adhesive wear mechanisms in the presence of weak interfaces: Insights from an amorphous model system. *Physical Review Materials,* 3**,** 053604.

BUDINSKI, K. G. 2011. Adhesive transfer to abrasive particles in abrasion testing. *Wear,* 271**,** 1258-1263.

BUDINSKI, K. G. & BUDINSKI, S. T. 2017. On replacing three-body abrasion testing with two-body abrasion testing. *Wear,* 376**,** 1859-1865.

CHANG, Y. H., JOO, B. S., LEE, S. M. & JANG, H. 2018. Size effect of tire rubber particles on tribological properties of brake friction materials. *Wear,* 394**,** 80-86.

CHINTHA, A., VALTONEN, K., KUOKKALA, V.-T., KUNDU, S., PEET, M. & BHADESHIA, H. 2019. Role of fracture toughness in impact-abrasion wear. *Wear*.

COATINGS, E. 2019. *Adhesive Wear Test ASTM G77* [Online]. Available: https://extremecoatings.net/technical-resources/test-results/adhesive-wear-test-astm-g77/.

COCKS, M. 1962. Interaction of sliding metal surfaces. *Journal of Applied Physics,* 33**,** 2152-2161.

DOERING, A., DANKS, D., MAHMOUD, S. & SCOTT, J. 2011. Evaluation of ASTM G65 abrasive—Spanning 13 years of sand. *Wear,* 271**,** 1252-1257.

FEREIDOUNI, H., AKBARZADEH, S. & KHONSARI, M. 2019. On the assessment of variable loading in adhesive wear. *Tribology International,* 129**,** 167-176.

FRÉROT, L., ANCIAUX, G. & MOLINARI, J.-F. 2019. Crack Nucleation in the Adhesive Wear of an Elastic-Plastic Half-Space. *arXiv preprint arXiv:1910.05163*.

GÅÅRD, A., HALLBÄCK, N., KRAKHMALEV, P. & BERGSTRÖM, J. 2010. Temperature effects on adhesive wear in dry sliding contacts. *Wear,* 268**,** 968-975.

GATES, J. 1998. Two-body and three-body abrasion: a critical discussion. *Wear,* 214**,** 139-146.

HAKAMI, F., PRAMANIK, A., ISLAM, N., BASAK, A. & RIDGWAY, N. 2019. Study of effective parameters on wear behavior of rubbers based on statistical methods. *Polymers for Advanced Technologies,* 30**,** 1415-1426.

HAKAMI, F., PRAMANIK, A., RIDGWAY, N. & BASAK, A. 2017. Developments of rubber material wear in conveyer belt system. *Tribology International,* 111**,** 148-158.

HOLMBERG, K. & ERDEMIR, A. 2019. The impact of tribology on energy use and CO2 emission globally and in combustion engine and electric cars. *Tribology International*.

HOLMBERG, K., KIVIKYTÖ-REPONEN, P., HÄRKISAARI, P., VALTONEN, K. & ERDEMIR, A. 2017. Global energy consumption due to friction and wear in the mining industry. *Tribology International,* 115**,** 116-139.

HUANG, M., GUIBERT, M., THÉVENET, J., FAYOLLE, C., CHAUSSÉE, T., GUY, L., VANEL, L., LOUBET, J.-L. & SOTTA, P. 2018. A new test method to simulate low-severity wear conditions experienced by rubber tire materials. *Wear,* 410**,** 72-82.

ISMAILOV, A., JÄRVELÄINEN, M. & LEVÄNEN, E. 2018. Problematics of friction in a high-speed rubber-wheel wear test system: A case study of irregularly rough steel in water lubricated contact. *Wear,* 408**,** 65-71.

KARSLI, N. G., YILMAZ, T. & GUL, O. 2018. Effects of coupling agent addition on the adhesive wear, frictional and thermal properties of glass fiber-reinforced polyamide 6, 6 composites. *Polymer Bulletin,* 75**,** 4429-4444.

KAYABA, T. & KATO, K. 1981. The adhesive transfer of the slip-tongue and the wedge. *Asle Transactions,* 24**,** 164-174.

KHAFIDH, M., SCHIPPER, D., MASEN, M., VLEUGELS, N., DIERKES, W. & NOORDERMEER, J. 2019. Friction and wear mechanism of short-cut aramid fiber and silica reinforced elastomers. *Wear,* 428**,** 481-487.

KOVAŘÍKOVÁ, I., SZEWCZYKOVÁ, B., BLAŠKOVIŠ, P., HODÚLOVÁ, E. & LECHOVIČ, E. 2009. Study and characteristic of abrasive wear mechanisms. *Materials Science and Technology,* 1**,** 1-8.

LAUX, K. A. 2016. *Adhesive Wear Phenomena in High Performance Polyaryletherketones (PAEK) Polymers.*

LI, Z., LI, Z. & WANG, Y. 2019. An Integrated Approach for Friction and Wear Simulation of Tire Tread Rubber. Part I: Friction Test, Characterization and Modeling. *Tire Science And Technology*.

LIN, L., ECKE, N., KAMERLING, S., SUN, C., WANG, H., SONG, X., WANG, K., ZHAO, S., ZHANG, J. & SCHLARB, A. K. 2018. Study on the impact of graphene and cellulose nanocrystal on the friction and wear properties of SBR/NR composites under dry sliding conditions. *Wear,* 414**,** 43-49.

LIU, T., KISER, M. T. & CLEMENTS, T. E. Effect of Microstructures on Low Stress Abrasive Wear of Steel Plates.

MAJUMDAR, J. D. & MANNA, I. 2015. Laser surface engineering of titanium and its alloys for improved wear, corrosion and high-temperature oxidation resistance. *Laser Surface Engineering.* Elsevier.

MECMESIN. 2018. *Peeling test in rubbers* [Online]. Available: https://www.mecmesin.com/test-type/peel.

MILANESE, E., AGHABABAEI, R., BRINK, T. & MOLINARI, J.-F. Surface roughness evolution in atomistic simulations of adhesive wear: from asperity collision to three-body configuration. Science of Wear Workshop, 2018a.

MILANESE, E., BRINK, T., AGHABABAEI, R. & MOLINARI, J.-F. Fractal surfaces in adhesive wear processes. 6th European Conference on Computational Mechanics European Conference on Computational Fluid Dynamics, 2018b.

MOLNAR, W., NEVOSAD, A., ROJACZ, H., ADAM, K., HENZE, H.-J., RIPOLL, M. R. & BADISCH, E. 2018. Two and three-body abrasion resistance of rubbers at elevated temperatures. *Wear,* 414**,** 174-181.

MOLNAR, W., VARGA, M., BRAUN, P., ADAM, K. & BADISCH, E. 2014. Correlation of rubber based conveyor belt properties and abrasive wear rates under 2-and 3-body conditions. *Wear,* 320**,** 1-6.

MUHR, A. & ROBERTS, A. 1992. Rubber abrasion and wear. *Wear,* 158**,** 213-228.

MUKHOPADHYAY, A. 2016. SEM study of worn surface morphology of an indigenous 'EPDM'rubber. *Polymer Testing,* 52**,** 167-173.

MYKIN. 2019. *Nitrile Rubber Specifications* [Online]. Available: https://mykin.com/nitrile-rubber-properties.

PAL, K., DAS, T., RAJASEKAR, R., PAL, S. K. & DAS, C. K. 2009. Wear characteristics of styrene butadiene rubber/natural rubber blends with varying carbon blacks by DIN abrader and mining rock surfaces. *Journal of applied polymer science,* 111**,** 348-357.

SASADA, T. 1984. Wear research in Japan: Trends and future directions. *Wear,* 100**,** 561-577.

SASAKI, S., SHIMA, M., NOGUCHI, S., HIRAYAMA, T., JIBIKI, T., ADACHI, K. & MIYAKE, K. 2013. A 1st Course in Tribology. Kodansha.

SCHALLAMACH, A. 1952. Abrasion of rubber by a needle. *Journal of polymer science,* 9**,** 385-404.

SHEN, M.-X., DONG, F., ZHANG, Z.-X., MENG, X.-K. & PENG, X.-D. 2016. Effect of abrasive size on friction and wear characteristics of nitrile butadiene rubber (NBR) in two-body abrasion. *Tribology International,* 103**,** 1-11.

SINGH, A. K. 2016. Assessment of mechanical and three-body abrasive wear peculiarity of TiO 2- and ZnO-filled bi-directional E-glass fibre-based polyester composites. *Bulletin of Materials Science,* 39**,** 971-988.

SINGH, A. K. & SIDDHARTHA 2015. Leverage of cenosphere filler size on mechanical and dry sliding wear peculiarity of polyester composites. *Journal of Composite Materials,* 49**,** 2789-2802.

SINGH GILL, N. & YOUSIF, B. 2009. Wear and frictional performance of betelnut fibre-reinforced polyester composite. *Proceedings of the Institution of Mechanical Engineers, Part J: Journal of Engineering Tribology,* 223**,** 183-194.

STACHOWIAK, G. B., SALASI, M., RICKARD, W. D. & STACHOWIAK, G. W. 2016. The effects of particle angularity on low-stress three-body abrasion-corrosion of 316L stainless steel. *Corrosion Science,* 111**,** 690-702.

TANGUDOM, P., THONGSANG, S. & SOMBATSOMPOP, N. 2014. Cure and mechanical properties and abrasive wear behavior of natural rubber, styrene–butadiene rubber and their blends reinforced with silica hybrid fillers. *Materials & design,* 53**,** 856-864.

TANZI, M. C., FARÈ, S. & CANDIANI, G. 2019. *Foundations of Biomaterials Engineering*, Academic Press.

TESTRESOURCES. 2018. *ASTM D429 Rubber to Metal Adhesion Test Equipment* [Online]. Available: https://www.testresources.net/applications/standards/astm/astm-d429-rubber-to-metal-adhesion-tests/.

WU, G. 2017. *The mechanisms of rubber abrasion.* Queen Mary University of London.

YOUSIF, B. 2013. Design of newly fabricated tribological machine for wear and frictional experiments under dry/wet condition. *Materials & Design,* 48**,** 2-13.

YOUSIF, B. F. 2012. Adhesive wear characteristics of natural fiber-reinforced composites.
ZHOU, C., CHEN, G., XIAO, S., HUA, Z. & GU, C. 2019. Study on fretting behavior of rubber O-ring seal in high-pressure gaseous hydrogen. *International Journal of Hydrogen Energy*.